biomass

MDPI

Article

Holistic Thermoenergetic Assessment of Biomass Boilers: An Integrated Static, Dynamic, and Emergy Framework

Eladio Omar Cajusol Pingo [1], Yoisdel Castillo Alvarez [1,*], Reinier Jiménez Borges [2], Jonny Paul Zavala de Paz [3], Francisco Antonio Castillo Velasquez [3,*], Luis Angel Iturralde Carrera [4] and Juvenal Rodríguez-Resendiz [4]

1 Department of Mechanical Engineering, Universidad Tecnológica del Perú, Lima 15046, Peru; u17210724@utp.edu.pe
2 Department of Mechanical Engineering, Faculty of Engineering, Universidad de Cienfuegos "Carlos Rafael Rodríguez", Cienfuegos 59430, Cuba; rjimenezborges@gmail.com
3 Industrial Technologies Division, Universidad Politécnica de Querétaro, Carretera Estatal 420 S/N, El Rosario, Queretaro 76240, Mexico; jonny.zavala@upq.edu.mx
4 Facultad de Ingeniería, Universidad Autónoma de Querétaro, Santiago de Querétaro 76010, Mexico; liturralde28@alumnos.uaq.mx (L.A.I.C.); juvenal@uaq.edu.mx (J.R.-R.)
* Correspondence: c19773@utp.edu.pe (Y.C.A.); francisco.castillo@upq.mx (F.A.C.V.)

Abstract

The evaluation of biomass boilers using partial approaches limits system understanding, because energy, exergy, dynamic, and emergy analyses describe complementary, but not equivalent, dimensions of thermo-industrial performance. In response to this gap, an integrated methodological framework is proposed to analyze two representative steam generator technologies in the sugar industry, fueled with ternary mixtures of sugarcane bagasse, Agricultural Crop Residues (ACR), and *Dichrostachys cinerea*, with the aim of identifying robust operating windows from a simultaneously thermal, exergetic, transient, and sustainability perspective. The methodology combines: (i) a direct and indirect steady-state model to quantify thermal losses and efficiency; (ii) an exergy model to assess conversion quality; (iii) a two-node coupled transient dynamic model capable of representing the differentiated response of the combustion zone and the water/steam system to moisture perturbations; and (iv) an emergy model to estimate the overall sustainability of the process. The results show that the effective moisture content of the mixture is the dominant control variable, since it determines the lower heating value on a wet basis, the specific fuel consumption, the main thermal loss, and the dynamic stability of the system. In the transient domain, a +5% step perturbation in moisture generates drops of 11.14–12.20 °C and 17.76–19.39 °C in furnace temperature for G1 and G2, respectively, while the steam response is damped to 1.03–1.14 °C and 2.39–2.65 °C. Likewise, moisture explains the magnitude of the response with coefficients of determination above 0.99, and the sensitivity analysis identifies the controller time constant, the thermal mass of the water/steam system, and the emissivity as the most influential parameters. Overall, the proposed framework makes it possible to go beyond isolated efficiency assessment and move toward a holistic characterization of biomass boiler performance under technically plausible ternary mixtures. Although the proposed methodological framework is transferable to other biomass combustion contexts, the numerical results—including optimal compositional zones, emergy indicators, and dynamic sensitivity coefficients—are specific to the Cuban sugar industry conditions, adopted transformities, and the biomass types evaluated herein.

Check for updates

Academic Editor: Jaehoon Kim

Received: 9 April 2026
Revised: 10 June 2026
Accepted: 15 June 2026
Published: 17 June 2026

Copyright: © 2026 by the authors. Licensee MDPI, Basel, Switzerland. This article is an open access article distributed under the terms and conditions of the Creative Commons Attribution (CC BY) license.

Keywords: biomass boilers; ternary biomass blends; emergy analysis; dynamic modeling; exergetic analysis

1. Introduction

The growing global energy demand, together with the urgent need to mitigate greenhouse gas emissions, has driven a progressive transition toward renewable energy sources [1]. In this context, biomass has emerged as one of the most promising resources for heat and power generation, since its combustion is considered approximately carbon-neutral when sustainably managed and it is the only renewable source capable of directly replacing solid fossil fuels in existing infrastructure [2,3]. At the global scale, biomass contributes more than 10% of primary energy, and this contribution is expected to grow significantly in the coming decades [4]. In sugar-producing countries such as Cuba, Brazil, India, and South Africa, sugarcane bagasse is the main biomass available for cogeneration in sugar mills, representing an on-site renewable resource generated as a by-product of milling [5,6].

However, bagasse typically has a moisture content between 45% and 55%, which significantly reduces its lower heating value (LHV) and, consequently, boiler efficiency [7,8]. Mo et al. [9] empirically showed that each 10% increase in bagasse moisture reduces thermal efficiency by 2–3 percentage points, establishing moisture as the factor with the greatest impact on boiler performance. This intrinsic limitation has motivated the exploration of blending strategies with complementary biomasses of higher energy density.

Among the complementary biomasses, *Dichrostachys cinerea* stands out as an invasive species widely distributed in Cuba, affecting approximately 7% of the country's cultivable land [10]. Its lower heating value (approximately 19,100 kJ/kg on a dry basis) is significantly higher than that of bagasse, and it has low chlorine and sulfur contents, making it suitable for direct combustion [11]. Reyes et al. [10] confirmed, through a comprehensive review of *Dichrostachys cinerea* thermochemical conversion processes, that this biomass exhibits properties comparable to or superior to those of established woody species, reinforcing its viability as a sustainable biofuel. Sugarcane agricultural crop residues (ACR), generated during mechanized harvest, constitute a second complementary source with relevant energy potential, although their higher ash content (5–6%) limits their participation in the blend to a maximum of approximately 20% to avoid wear and deposition problems in equipment [12,13]. Sagastume Gutiérrez et al. [14] evaluated the combined potential of bagasse, energy cane, and *Dichrostachys cinerea* for low-carbon electricity generation in Cuba, demonstrating that these biomasses can support more than 97% of the electricity generation planned by the Cuban government for 2030.

The combination of these biomasses in appropriate proportions makes it possible to optimize fuel properties, improve combustion stability, and extend cogeneration plant operating periods beyond the harvest season [15,16]. However, the performance evaluation of boilers fueled with biomass blends cannot be reduced to a single indicator or analysis method. Traditionally, studies have focused on partial approaches which, although valuable, do not fully capture the complexity of the system. The literature on biomass co-combustion has been oriented predominantly toward binary biomass-coal blends [17,18], with little attention to the exclusive combustion of ternary agricultural biomass mixtures, which represents a significant gap in the available knowledge.

Energy analysis based on the first law of thermodynamics has been the most widely used method to evaluate biomass boiler performance. This approach makes it possible to estimate thermal efficiency through the direct method—which relates the useful heat

transferred to steam to the energy supplied by the fuel—and through the indirect or loss method, which quantifies the different sources of energy losses according to ASME PTC 4-2008 and EN 12952-15 standards [19,20]. Cortes-Rodríguez et al. [7] conducted an experimental efficiency analysis of six bagasse boilers in sugar mills in the state of São Paulo (Brazil) using the indirect method, identifying fuel moisture as the main cause of energy losses of around 17–18%, with hot flue gas losses as the dominant component. Sosa-Arnao and Nebra [8] applied first- and second-law analysis to bagasse boilers, obtaining first-law efficiencies of 82–84% for 40–60 bar boilers, and showed that the method based on higher heating value (HHV) more clearly reveals the penalizing effect of moisture on efficiency.

Barroso et al. [21] developed an optimization model for RETAL-type boilers in Cuba based on the indirect method and a minimum total cost function, showing that operational adjustments—particularly the excess air coefficient and the stoichiometric ratio—can significantly increase efficiency. More recently, Molina et al. [22] combined indirect evaluation with multiobjective optimization using genetic algorithms for a 34 MW bagasse boiler in Colombia, achieving improvements of up to 0.8% in exergy efficiency (from 27.8% to 29.1%) and a reduction in bagasse consumption of 23 t/day. However, energy analysis alone has fundamental limitations: by relying exclusively on energy quantity, it does not distinguish between forms of energy with different thermodynamic quality, which can lead to an overestimation of the system's actual performance [23,24].

Exergy analysis, grounded in the first and second laws of thermodynamics, complements energy evaluation by considering not only the quantity but also the quality of energy, quantifying the maximum useful work obtainable from a flow relative to an environmental reference state and allowing identification of process irreversibilities [24,25]. In biomass boilers, exergy studies have consistently shown that the largest exergy destruction occurs in the combustion process, typically accounting for between 60% and 70% of the total exergy supplied by the fuel [26,27]. Compton and Rezaie [26] reported exergy efficiencies between 24% and 27% for biomass boilers (versus energy efficiencies of 76–85% in the same equipment), highlighting the fundamental gap between both indicators. Costa et al. [27], in a detailed study of a 50 MW biomass boiler in the Portuguese paper industry, constructed Sankey and Grassmann diagrams that revealed the main improvement opportunity lies in reducing the moisture content of residual biomass, since exergy losses associated with evaporation of water contained in the fuel are thermodynamically significant.

More advanced studies have incorporated the decomposition of exergy destruction into avoidable and unavoidable components, providing more precise information on priority improvement strategies. Tsatsaronis and Park [28] established the general theoretical framework for this decomposition in thermal systems, while Li et al. [29] applied it specifically to a real biomass boiler, determining that avoidable destruction is concentrated in the combustion chamber and heat transfer surfaces. Vučković et al. [30] extended this approach to industrial plants, finding that eliminating approximately 1 MW of avoidable exergy destruction in the steam boiler produces the greatest improvement in overall system efficiency. Together, these studies confirm that, although the energy efficiency of biomass boilers can reach acceptable values (75–90%), exergy efficiency rarely exceeds 30%, evidencing a wide margin for thermodynamic optimization.

Despite the usefulness of static models, they assume steady-state operating conditions that do not adequately reflect the real behavior of industrial boilers. In practice, biomass boilers experience continuous variations in fuel flow, moisture, steam demand, and other operating variables that significantly affect performance [9,31]. Dynamic modeling addresses this limitation by solving time-dependent mass and energy balances, allowing evaluation of the system's transient response to operating disturbances.

Mameri et al. [32] developed a 0D dynamic model based on the Bond Graph formalism for a 30 kW pellet boiler, successfully representing the transient behavior of the unit and determining that radiation is the dominant heat transfer mechanism in the combustion chamber, accounting for 97.6% of the total thermal transfer. Gómez et al. [33] presented an Eulerian CFD model for the transient simulation of pellet boilers, validated against experimental data on temperature and emissions, capturing the temporal evolution of bed combustion with spatial resolution. For circulating fluidized-bed boilers, Atsonios et al. [34] used the APROS platform to develop a validated 1D dynamic model that made it possible to study transient response to load changes, while Wang et al. [35], using the Modelica language, established a combined static-dynamic model of the dense zone of a 130 t/h biomass boiler, with relative errors below 3.8% with respect to real operational data. Carlon et al. [36], using TRNSYS for 6 and 12 kW boilers, reported better model-experiment agreement in steady state than in transient operation, underscoring the inherent difficulties in validating dynamic biomass boiler models.

Nevertheless, a transversal limitation of these works is that the dynamic modeling of biomass boilers has been developed separately from static exergy and energy analysis, without integrating the three perspectives into a unified methodological framework. Moreover, none of the cited models has been systematically applied to ternary biomass mixtures with variable composition, which represents a significant methodological gap.

Beyond thermodynamic efficiency, the integrated assessment of biomass-based energy systems requires considering the environmental sustainability of the process as a whole. Emergy analysis, developed by Odum [37,38], is a thermodynamically and ecologically grounded accounting framework that quantifies all energy, material, and service flows required to sustain a process, expressing them in a common unit: the solar emjoule (seJ). Unlike conventional energy analysis, which only accounts for energy available in the present moment, emergy evaluates the direct and indirect solar energy historically accumulated to generate a product or service, thereby providing a perspective of the system's "energy memory" [39,40].

Emergy indicators—such as the Emergy Yield Ratio (EYR), the environmental loading ratio (ELR), and the Emergy Sustainability Index (ESI)—allow simultaneous evaluation of the system's capacity to amplify economic inputs through local resource use, the environmental pressure exerted on the surrounding environment, and the long-term viability of the process [41,42]. Brown and Ulgiati [41] established that ESI values above 5 indicate long-term sustainable systems, while values below 1 suggest high dependence on non-renewable or imported resources. Hovelius and Hansson [43] conducted one of the first comparative studies applying energy, exergy, and emergy approaches simultaneously to biomass production, showing that each method captures different and complementary dimensions of system performance. More recently, Aghbashlo et al. [44] developed an integrated emergo-economic method to assess a municipal solid waste digestion plant equipped with a biogas engine, integrating thermodynamic, economic, and sustainability aspects. However, the combined application of emergy analysis with energy, exergy, and dynamic analyses to industrial biomass boilers remains scarcely explored in the literature.

The preceding review shows that energy, exergy, dynamic, and emergy approaches have been applied separately or, at best, in partial combinations (energy-exergy [8,26]; energy-emergy [43]; isolated dynamics [32,33,35,36]) for the evaluation of biomass systems. No studies were identified that systematically integrate these four perspectives into a unified methodological framework for boilers fueled with ternary biomass blends. This analytical fragmentation limits the holistic understanding of the system, since each approach captures only one dimension of performance: static energy analysis measures the quantity of energy utilized, exergy analysis evaluates thermodynamic quality, dynamic modeling re-

veals transient behavior, and emergy analysis quantifies environmental sustainability. Only through the integration of these perspectives is it possible to identify synergies, trade-offs, and improvement opportunities that remain hidden under partial approaches. As Maes and Van Passel [45] noted, exergy alone is insufficient as a sustainability indicator for bioenergy systems; the present work provides direct empirical evidence of this insufficiency by showing that exergy and emergy optima do not coincide for ternary biomass mixtures.

Accordingly, this work proposes an integrated methodological framework for the holistic thermoenergetic evaluation of biomass boilers, coherently combining: (i) a static direct and indirect model for energy efficiency; (ii) an exergy model for assessing conversion quality; (iii) a coupled two-node transient dynamic model for system response to operating variations; and (iv) an emergy model for environmental sustainability assessment. The framework is applied to ternary mixtures of sugarcane bagasse, sugarcane agricultural crop residues (ACR), and *Dichrostachys cinerea*, three biomasses of strategic relevance for the sugar industry in the Cuban and Caribbean context. Twelve ternary formulations are evaluated in two steam generator technologies (RETAL 45 t/h at 1.9 MPa and VU-40 235 t/h at 6.2 MPa), covering an effective moisture range of 35.5–40.75%. The results not only quantify the efficiency and sustainability of different blend configurations, but also identify optimal operating conditions from a multidimensional perspective that encompasses thermal performance, exergy quality, dynamic stability, and environmental viability.

The scientific contributions of this research are summarized below:

- An integrated methodological framework is proposed and numerically verified for internal consistency, coherently combining four analytical models (static energy, exergy, transient dynamics, and emergy) for the integrated, multidimensional evaluation of biomass boilers fueled with ternary mixtures—an approach that, to the authors' knowledge, has not been previously reported for boilers fired with ternary agricultural biomass blends.
- A coupled two-node transient dynamic model is developed that captures the differentiated thermal response of the combustion zone and the water/steam system to moisture perturbations, revealing a technology-dependent thermal damping factor ($\approx$10.9$\times$ for the RETAL generator and $\approx$7.4$\times$ for the VU-40) not previously quantified for industrial bagasse boilers, with steam temperature deviations below 3 °C under +5% moisture perturbations.
- Through cross-model statistical analysis (linear regression with $R^2 > 0.99$, OAT sensitivity, and Monte Carlo simulation with $N = 2000$), it is demonstrated that effective mixture moisture is the dominant structural control variable governing thermal efficiency, exergy performance, and dynamic stability simultaneously.
- The multidimensional conflict between thermal, exergy, and emergy optima is identified and quantified—with Spearman correlation $\rho = -0.182$ ($p = 0.572$, $n = 12$) between thermal and emergy rankings—providing preliminary statistical indication that thermal efficiency and emergy sustainability rankings are not significantly correlated, suggesting that no single-dimensional optimization criterion is sufficient for robust biomass mixture selection within the evaluated compositional space.
- Reference data are provided for the Cuban sugar industry on the performance of 12 ternary bagasse: ACR: *Dichrostachys cinerea* mixtures in two steam generator technologies, including $d\eta_{th}/dW$ sensitivities and dynamic deviation slopes, which were not previously available in the literature.

This paper is organized as follows. Section 1, Introduction, presents the energy, exergy, dynamic, and emergy assessment context for biomass boilers and identifies the methodological gap addressed in this work. Section 2, Materials and Methods, describes the integrated framework, the ternary biomass mixtures considered, the boiler operating

conditions, and the formulation of the four models used in the study. Section 3, Results, reports the thermal, exergy, dynamic, and emergy performance of the 12 mixtures evaluated in the two steam generators. Section 4, Discussion, analyzes the main findings in relation to the literature and highlights the multidimensional trade-offs among efficiency, stability, and sustainability. Finally, Section 5, Conclusions, summarizes the principal contributions, limitations, and implications of the proposed framework.

2. Materials and Methods

Table 1 shows the moisture ranges and the measured physicochemical properties of the different biomasses evaluated in this study. Key parameters such as the lower heating value (LHV) and the elemental composition in terms of carbon (C), hydrogen (H), oxygen (O), nitrogen (N), sulfur (S), and ash content are included. These data are essential for characterizing the energy potential and quality of each biomass type, thereby enabling an appropriate comparison and selection for energy conversion processes. In addition, the table shows how these properties vary with different moisture levels, which is crucial for understanding their behavior and efficiency in thermal or combustion applications.

Table 1. Reference physicochemical properties of the evaluated biomasses at different moisture contents.

Biomass	Moisture (%)	LHV (kJ/kg)	C (%)	H (%)	O (%)	N (%)	S (%)	Ash (%)
Bagasse	45	8500.0	42.5	5.3	35.1	0.4	0.05	3.1
	50	7800.0	42.1	5.3	36.2	0.4	0.05	3.1
	55	7240.4	41.98	5.28	36.17	0.41	0.05	3.12
	60	6200.0	41.6	5.2	36.6	0.4	0.05	3.1
ACR	10	15,800.0	37.4	4.9	37.5	0.2	0.05	5.1
	15	14,774.45	37.15	4.89	37.67	0.19	0.05	5.06
	20	13,500.0	36.9	4.9	37.8	0.2	0.05	5.1
	25	12,000.0	36.7	4.9	38.0	0.2	0.05	5.1
	30	11,200.0	36.5	4.9	38.2	0.2	0.05	5.1
Dichrostachys cinerea	5	17,000.0	46.4	3.3	49.3	0.6	0.49	0
	10	16,900.0	46.4	3.3	49.3	0.6	0.49	0
	15	16,700.0	46.4	3.3	49.3	0.6	0.49	0
	20	16,400.0	46.4	3.3	49.3	0.6	0.49	0
	25	16,000.0	46.4	3.3	49.3	0.6	0.49	0
	30	15,923.06	46.34	3.33	49.28	0.56	0.49	0

2.1. Mixture Selection

The appropriate selection of the proportion of each biomass in the blend is essential to optimize energy efficiency and minimize operational problems in the boiler. Industrial practice typically limits ACR participation to approximately 20% in boilers designed exclusively for bagasse combustion, due to the higher ash content of ACR (5–6% vs. 3.1% for bagasse) and the associated risks of slagging and tube deposition [7,8]. However, for the spreader-stoker grate configurations characteristic of RETAL and VU-40 generators, which feature continuous ash removal and were originally designed to tolerate fuel variability during harvest operations, ACR fractions up to 30% have been evaluated in operational trials without reportable deposition incidents [46]. The ash fusion temperature of Cuban ACR (>1100 °C) exceeds typical furnace wall temperatures, providing an additional safety margin.

2.2. Static Thermoenergetic Model: Blend Properties, Energy, and Exergy Efficiency

The integrated framework combines four models: a static energy model, an exergy model, a transient two-node dynamic model, and an emergy model. The static energy and exergy formulations and the blend-property mixing rules rely on standard expressions widely established in the literature; for conciseness they are summarized below in prose and reported in full, together with their nomenclature, in the Supplementary Material. The non-

standard core of the framework—the coupled two-node transient model—is developed in detail in the main text (Section 2, Equations (2)–(9)).

Blend moisture (W_{blend}), lower heating value, and average elemental composition were computed as mass-weighted averages of the component properties for $n = 3$ components (bagasse, ACR, and *Dichrostachys cinerea*), using the base properties at the reference moisture conditions reported in Table 1 (Supplementary Material, Equation (S1)). The wet-basis lower heating value follows from the dry-basis value and the effective moisture fraction:

$$LHV_{\text{wet}} = LHV_{\text{dry}} \times (1 - W_{\text{blend}}). \quad (1)$$

Thermal efficiency was computed by both the direct method—the ratio of useful heat transferred to the steam ($Q_{\text{useful}} = \dot{m}_v(h_v - h_a)$) to the fuel energy input ($Q_{\text{comb}} = \dot{m}_f$ LHV)—and the indirect or loss method ($\eta_{\text{th,ind}} = 100 - \sum q_i$, with hot-gas, incombustion, and radiation/convection losses q_2–q_6 after ASME PTC 4 and EN 12952-15). Exergy efficiency was obtained as the ratio of the useful steam exergy ($Ex_v = \dot{m}_v[(h_v - h_a) - T_0(s_v - s_a)]$) to the fuel exergy ($Ex_f = \dot{m}_f\, ex_f$), with the fuel specific exergy ex_f estimated from its LHV and elemental composition through a standard Szargut-type correlation. The complete set of static expressions (Equations (S2)–(S4)) and the corresponding variable definitions (Table 2) are given in the Supplementary Material.

Table 2. Description of variables.

Variable	Description	Unit
C, H, O, S, W	Elemental composition of the biomass (dry or wet basis)	[%]
$\dot{m}_f$	Mass flow rate of fed biomass	[kg/h]
$\dot{m}_v$	Mass flow rate of generated steam	[kg/h]
h_v, h_a	Enthalpy of steam and feedwater	[kJ/kg]
h, h_0, s, s_0	Thermodynamic and exergy parameters	[kJ/kg], [kJ/kg·K]
T_0	Ambient temperature (exergy reference)	[K]
q_2 to q_6	Thermal losses (indirect method)	[%]

2.3. Dynamic Model (Transient–System Temporal Response)

This section introduces a dynamic model that analyzes the system's temporal response to variations in operating conditions, such as changes in fuel flow or moisture content. Through transient energy balance (2), the evolution of steam temperature over time is evaluated, incorporating thermal losses and other relevant variables for a more realistic and detailed analysis of system behavior.

2.3.1. General Energy Balance Equation

$$\frac{dT_{\text{steam}}}{dt} = f\Big(Q_{\text{comb}}(t),\ \dot{m}_f(t),\ W(t),\ \text{other variables}\Big) \quad (2)$$

where:

- $\frac{dT_{\text{steam}}}{dt}$: Steam temperature variation rate [°C/h or K/h].
- $Q_{\text{comb}}(t)$: Instantaneous energy supplied by the fuel [kW].
- $\dot{m}_f(t)$: Fuel mass flow rate at time t [kg/h].
- $W(t)$: Fuel moisture content [%].
- Other variables: Thermal losses, water flow, changing operating conditions, etc.

2.3.2. Expanded Form of the Energy Balance

The expanded energy balance Equation (3) explicitly incorporates thermal inertia of the steam generator through the product of total water/steam mass (M) and average specific heat (C_p), relating the rate of steam temperature change to instantaneous combustion input, environmental losses, and useful heat extraction.

$$M \cdot C_p \cdot \frac{dT_{\text{steam}}}{dt} = Q_{\text{comb}}(t) - Q_{\text{losses}}(t) - Q_{\text{useful}}(t) \quad (3)$$

where:

- M: Total water/steam mass in the generator [kg].
- C_p: Average specific heat of the system [kJ/kg·K].
- $Q_{\text{losses}}(t)$: Instantaneous heat lost to the environment [kW].
- $Q_{\text{useful}}(t)$: Useful heat transferred to steam [kW].

This equation enables analysis of the system's thermal response to changes in operating conditions, such as fuel feeding, moisture content, or steam extraction.

2.4. Physical Definition of the Model Nodes

The proposed dynamic model decomposes the steam generator into two coupled thermal zones, each treated as an independent control volume with thermal storage capacity. This decomposition is based on the structural and operational differences between the zone where energy is released by combustion and the zone where that energy is transferred to the working fluid.

2.4.1. Node 1—Combustion Zone (Furnace)

Node 1 physically represents the combustion chamber of the steam generator, including: (i) the combustion bed where biomass is oxidized on the grate or in suspension through the spreader-stoker system, (ii) the hot combustion gases that fill the furnace volume, (iii) the refractory walls lining the chamber internally, and (iv) the fly ash suspended in the gases. In thermodynamic terms, this node stores thermal energy in the refractory mass and gases, and releases it through two heat-transfer mechanisms toward Node 2: radiation from the flame and hot gases to the water walls, and convection from the gases to the tube banks downstream of the furnace.

The effective thermal mass of this node (M_1) is relatively small—on the order of 3500 kg for the RETAL 45 t/h generator and 8000 kg for the VU-40 235 t/h generator—because the combustion gases have low density and the refractory, although dense, has a limited volume. This low thermal inertia implies that any change in fuel quality (moisture, calorific value) is rapidly reflected in the furnace temperature, with effective time constants on the order of 2–5 min.

2.4.2. Node 2—Water/Steam System

Node 2 represents the system where thermal energy from the furnace is transferred to the working fluid to produce steam. It includes: (i) the water walls that receive direct radiation from the furnace, (ii) the tubes of the convective bank that receive heat from the hot gases, (iii) the upper drum where steam is separated from the water-steam mixture, (iv) the superheater where saturated steam is raised to its final temperature, and (v) the economizer where feedwater is preheated by the exhaust gases.

The thermal mass of this node (M_2) is considerably greater than that of Node 1—on the order of 32,000 kg for the RETAL and 142,000 kg for the VU-40—since it includes several thousand kilograms of liquid water and steam in the circuit, plus the metal mass of the tubes, drums, and headers. The ratio M_2/M_1 ranges from 9 to 18 depending on

the technology, which gives Node 2 a high thermal inertia that damps perturbations from the furnace before they affect the temperature of the produced steam. The strength of this damping is not governed by the bare mass ratio M_2/M_1 alone, but by the thermal capacitance of Node 2 relative to its useful heat extraction (M_2/Q_{useful}), as analysed in the dynamic results.

2.4.3. Governing Equations of the Two-Node Model

The model starts from Equation (4) of the manuscript, which states the global transient energy balance of the generator as a single control volume:

$$M \cdot C_p \cdot \frac{dT_{\text{vapor}}}{dt} = Q_{\text{comb}}(t) - Q_{\text{loss}}(t) - Q_{\text{useful}}(t) \tag{4}$$

The decomposition of this balance into two coupled nodes (5) and (6) leads to the following equations, which are direct applications of the first law of thermodynamics to each subvolume:

$$M_1 \cdot C_{p1} \cdot \frac{dT_1}{dt} = Q_{\text{comb}}(t) - Q_{\text{rad}}(T_1, T_2) - Q_{\text{conv}}(T_1, T_2) - Q_{\text{gases}}(t) \tag{5}$$

$$M_2 \cdot C_{p2} \cdot \frac{dT_2}{dt} = Q_{\text{rad}}(T_1, T_2) + Q_{\text{conv}}(T_1, T_2) - Q_{\text{useful}} - Q_{\text{ext}} \tag{6}$$

The coupling between nodes (7) and (8) is achieved through radiative and convective heat transfer:

$$Q_{\text{rad}} = \sigma \cdot \varepsilon \cdot A_{\text{rad}} \cdot \left(T_1^4 - T_2^4\right) \tag{7}$$

$$Q_{\text{conv}} = UA \cdot (T_1 - T_2) \tag{8}$$

where $\sigma = 5.67 \times 10^{-8}$ W/m^2·K^4 is the Stefan–Boltzmann constant, ε is the effective emissivity of the biomass flame (nominal value $\varepsilon = 0.45$), A_{rad} is the area of the water walls exposed to radiation, and UA is the product of the overall convective heat-transfer coefficient and the area of the tube banks. These four equations form a system of two coupled nonlinear ordinary differential equations (due to the T^4 term in radiation), which is solved numerically by explicit Euler integration with a time step of $dt = 0.002$ h (7.2 s).

It is important to verify that this decomposition preserves thermodynamic consistency: by summing Equations (5) and (6), the Q_{rad} and Q_{conv} terms cancel as internal transfers between the two subvolumes, and Equation (4) is recovered exactly, with $M \cdot C_p = M_1 \cdot C_{p1} + M_2 \cdot C_{p2}$ and $Q_{\text{loss}} = Q_{\text{gases}} + Q_{\text{ext}}$.

2.4.4. Simulated Perturbation

A step perturbation of +5% absolute in fuel moisture was applied at $t = 0$. This magnitude was selected because it represents a realistic operational fluctuation in sugarcane bagasse moisture during the harvest season, where moisture may vary between 45–55% depending on milling conditions, storage time, and climatic conditions. The +5% step is a moderate-to-severe disturbance scenario that allows evaluation of the system's buffering capacity without exceeding safe operating limits.

The perturbation generates two simultaneous effects: (i) an instantaneous drop in the lower heating value on a wet basis of the fuel ($\text{LHV}_{\text{new}} = \text{LHV}_{\text{dry}} \times (1 - W_{\text{new}})$), and (ii) a gradual increase in fuel mass flow rate ($\dot{m}_f$) as the response of the feeding control system, modeled as a first-order lag with time constant τ (nominal value $\tau = 5.5$ min) (9):

$$\dot{m}_f(t) = \dot{m}_{f,\text{nom}} + \left(\dot{m}_{f,\text{new}} - \dot{m}_{f,\text{nom}}\right)\left(1 - e^{-t/\tau}\right) \tag{9}$$

The sensitivity dq_2/dW used to calculate the new losses was obtained by direct linear regression ($dq_2/dW = 0.212\%/\%$ for G1, $0.161\%/\%$ for G2).

2.5. Emergy Model (Environmental Sustainability, EMERGY)

Emergy modeling includes the definition of the system's spatio-temporal boundaries, the emergy modeling itself, and the determination of fundamental indicators from established and/or calculated transformities.

2.5.1. Spatio-Temporal Boundaries of the System

Thermodynamic systems are defined as any spatial region within a prescribed boundary selected for study, which must be established for a specific time period since this factor defines the flows crossing the system. In the present work, the system boundary encompasses the steam-generation process from biomass reception to useful steam delivery; the harvesting and milling stages of bagasse production are accounted for through the purchased economic flows—materials (M) and services (S)—and are therefore not excluded from the analysis. This stage specifies the object of analysis and the time period for evaluation. Failure to properly establish these variables can lead to errors in quantifying the inputs and outputs consumed and provided by the system, respectively.

2.5.2. Emergy Modeling

This step consists of representing flows of matter and energy using emergy symbology to illustrate interactions between internal and external sources of the system, as well as output flows and feedback. The main function is data organization, enabling identification of system flows and interactions, highlighting the most relevant ones. Scale and level of detail may vary depending on objectives and socio-ecosystem type.

The modeling comprises the following steps:

- From system boundaries, main energy inputs and outputs are defined and classified by nature (biogeophysical, economic, human, etc.), ordered left to right by increasing transformity around the system boundary symbol.
- Internal system components and their relationships with matter/energy inputs/outputs and among themselves are defined, ensuring inclusion of all elements regulating processes constituting system functioning, following the same ordering criterion.
- Monetary flows corresponding to economic use of some system flows are included, such as money inputs driving socioeconomic components.
- Energy degradation corresponding to the second law of thermodynamics is incorporated.
- The diagram is simplified according to study objectives by aggregating categories to the desired level of detail.

2.5.3. Construction of Emergy Tables

Starting from the energy-exergy balance, the emergy table construction proceeds. As shown in Table 3, the first column presents the order of each flow and its origin. The second column shows flow names; the third, calculated values for each flow; the fourth, their units; the fifth, emergy per unit (transformity or specific emergy) converting column 3 values to solar emergy; and the sixth, corresponding total solar emergy.

Table 3. Typical example of an emergy table.

Note	Item	Data	Unit	Transformity (seJ/Unit)	Solar Emergy (seJ/Year)
1	Item 1	Value 1	J/year	Transformity 1	Em1
2	Item 2	Value 2	g/year	Transformity 2	Em2
⋮	⋮	⋮	⋮	⋮	⋮
n	Item n	Value n	J/year	Transformity n	Emn
Y	Y-th product	Data Y	J or g/year	$\sum_{i=1}^{n} E_{mi}$/Item	$\sum_{i=1}^{n} E_{mi}$

Emergy evaluation follows Odum and Brown principles, considering all input and output flows of the biomass-fed steam generator system. The calculation develops through the following stages:

2.5.4. Emergy Indicators and Goodness-of-Fit Metrics

The emergy of each flow was obtained as the product of the quantity used and its corresponding transformity, and the flows were aggregated into renewable (R), non-renewable (N), and economic (F) emergy—the economic emergy comprising purchased materials (M) and services (S), $F = M + S$—with the total invested emergy $U = R + N + F$. From these, the standard emergy indicators were computed: the transformity (U/Q_{useful}), the emergy yield ratio (EYR $= U/F$), the environmental loading ratio (ELR $= (N + F)/R$), the emergy sustainability index (ESI $=$ EYR/ELR), and the renewability percentage ($\%R = R/U \times 100$). The agreement between simulated and reference steam temperatures, where applicable, was quantified through the mean absolute error (MAE), root-mean-square error (RMSE), mean absolute percentage error (MAPE), and coefficient of determination (R^2). All these standard expressions, together with their full nomenclature, are reported in the Supplementary Material (Equations (S5)–(S8)).

3. Results

The results were structured to establish a direct relationship between the composition of the ternary bagasse–ACR–*Dichrostachys cinerea* mixtures and the thermoenergetic response of the two evaluated steam generators. To this end, the analysis was developed sequentially, starting from the global characterization of the selected mixtures and progressing toward quantification of their effect on system performance variables. First, the influence of the mass proportion of each component on the effective fuel moisture content and its lower heating value on a wet basis was examined, as both parameters decisively condition fuel requirements, the magnitude of thermal losses, and generator operating efficiency.

Building on this physicochemical foundation, the behavior of each mixture was comparatively evaluated in the two generation technologies considered, with emphasis on the variation of dominant losses and their impact on indirect thermal efficiency and system exergy response. This approach enabled identification of performance sensitivity to moderate changes in fuel composition while simultaneously delineating the mixture region with greatest improvement potential under technically realistic operating conditions. Consequently, the results are not presented as isolated values, but as part of a causal sequence linking composition, fuel properties, and overall generator performance.

To more faithfully represent plausible biomass energy utilization operating conditions, a ternary mixture matrix was defined, restricted to a technically viable compositional region, avoiding extreme formulations while preserving bagasse as the structurally dominant or quasi-dominant fuel component. This experimental delimitation focused the analysis on industrially relevant combinations where ACR and *Dichrostachys cinerea* fractions act as modifiers of effective moisture content and mixture calorific value without denaturing the bagasse-based system character. Accordingly, the present study evaluates ACR fractions

of 15–30% to cover both the conventional operational window (≤20%) and a technically feasible extended range (25–30%), thereby enabling a more comprehensive characterization of the compositional space. Mixtures with ACR > 20% are classified as "adjusted ternary" formulations in Table 4, while those within the conventional range are classified as "conservative ternary".

Table 4. Definition of evaluated cases according to adjusted ternary mixture composition and steam generator type.

Case	Mix ID	Bagasse (%)	ACR (%)	*Dichrostachys cinerea* (%)	Mixture Type	Use in Manuscript	Generator
C1	M1	50	30	20	Adjusted ternary	Main body	G1–RETAL 45 t/h
C2	M1	50	30	20	Adjusted ternary	Main body	G2–235 t/h, 80 bar, 450 °C
C3	M2	50	25	25	Adjusted ternary	Main body	G1–RETAL 45 t/h
C4	M2	50	25	25	Adjusted ternary	Main body	G2–235 t/h, 80 bar, 450 °C
C5	M3	55	30	15	Adjusted ternary	Main body	G1–RETAL 45 t/h
C6	M3	55	30	15	Adjusted ternary	Main body	G2–235 t/h, 80 bar, 450 °C
C7	M4	55	25	20	Adjusted ternary	Main body	G1–RETAL 45 t/h
C8	M4	55	25	20	Adjusted ternary	Main body	G2–235 t/h, 80 bar, 450 °C
C9	M5	60	30	10	Conservative ternary	Main body	G1–RETAL 45 t/h
C10	M5	60	30	10	Conservative ternary	Main body	G2–235 t/h, 80 bar, 450 °C
C11	M6	55	20	25	Adjusted ternary	Main body	G1–RETAL 45 t/h
C12	M6	55	20	25	Adjusted ternary	Main body	G2–235 t/h, 80 bar, 450 °C
C13	M7	60	25	15	Conservative ternary	Main body	G1–RETAL 45 t/h
C14	M7	60	25	15	Conservative ternary	Main body	G2–235 t/h, 80 bar, 450 °C
C15	M8	60	20	20	Conservative ternary	Main body	G1–RETAL 45 t/h
C16	M8	60	20	20	Conservative ternary	Main body	G2–235 t/h, 80 bar, 450 °C
C17	M9	65	25	10	Conservative ternary	Main body	G1–RETAL 45 t/h
C18	M9	65	25	10	Conservative ternary	Main body	G2–235 t/h, 80 bar, 450 °C
C19	M10	60	15	25	Conservative ternary	Main body	G1–RETAL 45 t/h
C20	M10	60	15	25	Conservative ternary	Main body	G2–235 t/h, 80 bar, 450 °C
C21	M11	65	20	15	Conservative ternary	Main body	G1–RETAL 45 t/h
C22	M11	65	20	15	Conservative ternary	Main body	G2–235 t/h, 80 bar, 450 °C
C23	M12	65	15	20	Conservative ternary	Main body	G1–RETAL 45 t/h
C24	M12	65	15	20	Conservative ternary	Main body	G2–235 t/h, 80 bar, 450 °C

Once the study cases were established, the global properties of each mixture were estimated through mass-weighted balances from the base properties of their three components. Accordingly, Table 5 summarizes the estimated properties of the selected bagasse:ACR:*Dichrostachys cinerea* mixtures, constituting the physicochemical input basis for subsequent comparative steam generator evaluation.

Table 5. Estimated properties of selected Bagasse:ACR:*Dichrostachys cinerea* mixtures under different mass proportions.

ID	Bagasse:ACR:*Dichrostachys cinerea* Mixture (%)	Mixture Moisture (%)	LHV Mixture (kJ/kg)	C (%)	H (%)	O (%)	N (%)	S (%)	Ash (%)
M1	50:30:20	35.50	11,516.95	41.463	4.783	39.257	0.369	0.138	3.592
M2	50:25:25	36.25	11,574.38	41.922	4.705	39.838	0.388	0.160	3.470
M3	55:30:15	36.50	11,110.79	41.251	4.881	38.603	0.361	0.116	3.616
M4	55:25:20	37.25	11,168.23	41.711	4.804	39.184	0.380	0.138	3.494
M5	60:30:10	37.50	10,704.64	41.039	4.980	37.949	0.353	0.094	3.640
M6	55:20:25	38.00	11,225.66	42.170	4.726	39.764	0.398	0.160	3.372
M7	60:25:15	38.25	10,762.07	41.498	4.902	38.529	0.371	0.116	3.518
M8	60:20:20	39.00	10,819.50	41.958	4.824	39.110	0.390	0.138	3.396
M9	65:25:10	39.25	10,355.92	41.287	5.000	37.876	0.363	0.094	3.542
M10	60:15:25	39.75	10,876.93	42.418	4.746	39.691	0.408	0.160	3.274
M11	65:20:15	40.00	10,413.35	41.746	4.923	38.456	0.382	0.116	3.420
M12	65:15:20	40.75	10,470.78	42.206	4.845	39.037	0.400	0.138	3.298

Note: Mixture properties were estimated by mass-weighted averages from base properties of bagasse, ACR, and *Dichrostachys cinerea*, using the formulation $W_{\text{mixture}} = \sum x_i W_i$ and $\text{LHV}_{\text{mixture}} = \sum x_i \text{LHV}_i$, consistent with the manuscript calculation scheme.

Thermoenergetic and exergy evaluation of the mixtures requires fixing beforehand the operating conditions of the steam generators and boundary thermodynamic parameters used in the balances. Accordingly, Table 6 consolidates in a single matrix the technical and thermodynamic data used in calculations.

From the estimated physicochemical properties of the ternary mixtures and the operating conditions established for both steam generators, their thermal performance was evaluated using the indirect method. Under this approach, Table 7 summarizes the thermal behavior of the selected mixtures, integrating global fuel moisture content, LHV, and each technology's response in terms of q_2 and indirect thermal efficiency ($\eta_{\text{th,ind}}$).

Table 6. Operating and thermodynamic parameters adopted for the evaluated steam generators.

Parameter	Symbol	G1–RETAL Steam Generator	G2–High-Parameter Steam Generator
Nominal steam generation capacity	D_v	45 t/h	235 t/h
Operating steam generation used in calculations	$\dot{m}_v$	45,000 kg/h	213,200 kg/h
Design pressure	P_{design}	—	8.0 MPa
Operating pressure	P	1.9 MPa	6.2 MPa
Steam temperature	T_v	320 °C	450 °C
Operating steam temperature used in calculations	$T_{v,\text{calc}}$	320 °C	455.5 °C
Feedwater temperature	T_{aa}	80 °C	137.8 °C
Steam enthalpy	h_v	3045 kJ/kg	3315 kJ/kg
Feedwater enthalpy	h_a	335 kJ/kg	579 kJ/kg
Steam entropy	s_v	6.85 kJ/kg·K	6.78 kJ/kg·K
Feedwater entropy	s_a	1.08 kJ/kg·K	1.66 kJ/kg·K
Boiler outlet excess-air coefficient	α_{gsal}	2.0	2.0
Furnace outlet excess-air coefficient	α_H	1.8	1.8
Flue-gas outlet temperature	T_{gsal}	213.74 °C	179.3884 °C
Reference temperature	T_0	298.15 K	298.15 K
Reference pressure	P_0	1.013 bar	1.013 bar
Nominal external-cooling heat loss	$q_{5,\text{nom}}$	1.0 %	0.6 %

Note: Parameters included in this table constitute the adopted operational and thermodynamic basis for comparative evaluation of both generators.

Table 7. Thermal performance of selected Bagasse:ACR:*Dichrostachys cinerea* mixtures for the evaluated steam generators.

Mixture B:A:M (%)	Mixture Moisture (%)	LHV Mixture (kJ/kg)	q_2 RETAL (%)	$\eta_{\text{th,ind}}$ RETAL (%)	q_2 VU-40 (%)	$\eta_{\text{th,ind}}$ VU-40 (%)	η Average (%)
50:30:20	35.50	11,516.95	15.86	81.19	11.22	86.49	83.84
50:25:25	36.25	11,574.38	15.99	81.06	11.32	86.39	83.73
55:30:15	36.50	11,110.79	16.10	80.95	11.40	86.31	83.63
55:25:20	37.25	11,168.22	16.23	80.82	11.50	86.21	83.52
60:30:10	37.50	10,704.64	16.34	80.71	11.58	86.13	83.42
55:20:25	38.00	11,225.66	16.36	80.69	11.60	86.11	83.40
60:25:15	38.25	10,762.07	16.47	80.58	11.68	86.03	83.31
60:20:20	39.00	10,819.50	16.60	80.45	11.78	85.93	83.19
65:25:10	39.25	10,355.92	16.71	80.34	11.86	85.85	83.09
60:15:25	39.75	10,876.93	16.72	80.33	11.88	85.83	83.08
65:20:15	40.00	10,413.35	16.84	80.21	11.96	85.75	82.98
65:15:20	40.75	10,470.78	16.96	80.09	12.06	85.65	82.87

The results show a clear monotonic trend: as mixture moisture increases, q_2 increases and indirect thermal efficiency decreases in both generators. This behavior indicates that effective fuel moisture acts as the dominant control variable for thermal performance, penalizing available heat utilization and increasing combustion gas losses.

Within the evaluated window, mixture 50:30:20 exhibited the best overall performance, with 81.19% in the RETAL generator, 86.49% in the VU-40, and average efficiency of 83.84%. This is followed by mixtures 50:25:25 and 55:30:15, confirming that the region of greatest thermal interest concentrates in compositions with 50–55% bagasse, 25–30% ACR, and 15–25% *Dichrostachys cinerea*. In contrast, mixtures with higher bagasse fraction and moisture content, such as 65:15:20, show the lowest efficiency values.

Likewise, the VU-40 generator maintains superior efficiencies to RETAL across all analyzed mixtures, with a systematic difference on the order of 5 percentage points. However, the relative mixture ranking remains consistent across both technologies, demonstrating that fuel composition effects are robust against generator changes.

Table 8 presents the exergy performance of the selected ternary mixtures in both steam generators.

Table 8. Specific fuel exergy, exergy flow, and exergy efficiency for evaluated Bagasse:ACR: *Dichrostachys cinerea* mixtures.

Mixture B:A:M (%)	ex_f Specific (kJ/kg)	Ex_f RETAL (kJ/h)	Ex_v RETAL (kJ/h)	η_{ex} RETAL (%)	Ex_f VU-40 (kJ/h)	Ex_v VU-40 (kJ/h)	η_{ex} VU-40 (%)	η_{ex} Average (%)
50:30:20	12,928.74	136,899,100.00	44,535,352.50	32.53	654,820,220.55	257,859,430.40	39.38	35.96
50:25:25	12,988.95	136,854,162.22	44,535,352.50	32.54	654,605,272.68	257,859,430.40	39.39	35.97
55:30:15	12,471.52	136,885,127.90	44,535,352.50	32.53	654,753,388.75	257,859,430.40	39.38	35.96
55:25:20	12,531.90	136,840,433.86	44,535,352.50	32.54	654,539,606.75	257,859,430.40	39.40	35.97
60:30:10	12,014.44	136,871,570.10	44,535,352.50	32.54	654,688,538.64	257,859,430.40	39.39	35.96
55:20:25	12,592.27	136,796,176.23	44,535,352.50	32.56	654,327,912.22	257,859,430.40	39.41	35.98
60:25:15	12,074.90	136,826,251.39	44,535,352.50	32.55	654,471,768.72	257,859,430.40	39.40	35.97
60:20:20	12,135.40	136,781,919.52	44,535,352.50	32.56	654,259,719.07	257,859,430.40	39.41	35.99
65:25:10	11,617.98	136,811,864.29	44,535,352.50	32.55	654,402,951.85	257,859,430.40	39.40	35.98
60:15:25	12,195.94	136,738,503.16	44,535,352.50	32.57	654,052,048.52	257,859,430.40	39.42	36.00
65:20:15	11,678.67	136,768,067.20	44,535,352.50	32.56	654,193,460.23	257,859,430.40	39.42	35.99
65:15:20	11,739.34	136,724,583.74	44,535,352.50	32.57	653,985,468.70	257,859,430.40	39.43	36.00

The results show that moisture remains the control variable, but its effect on exergy efficiency is more moderate than on thermal efficiency. As mixture moisture increases, wet-basis LHV decreases, required fuel exergy (Ex_f) increases, and since useful steam exergy (Ex_v) remains constant for each generator, exergy efficiency (η_{ex}) decreases slightly. The total range of average exergy efficiency across all 12 mixtures is only 0.04 percentage points (35.96–36.00%), so η_{ex} is effectively invariant with respect to mixture composition within the evaluated window.

3.1. Dynamic Model Results

3.1.1. Transient Response of Node 1 (Combustion Zone)

Furnace temperature (T_1) is the first variable responding to fuel moisture changes, as the furnace represents direct contact between fuel and energy release process. Response rapidity is determined by the low thermal mass of refractory and gases (M_1), enabling rapid transfer of energy deficit caused by increased moisture. Figure 1 presents the temporal evolution of T_1 for four representative mixtures covering the evaluated compositional range, for both steam generators.

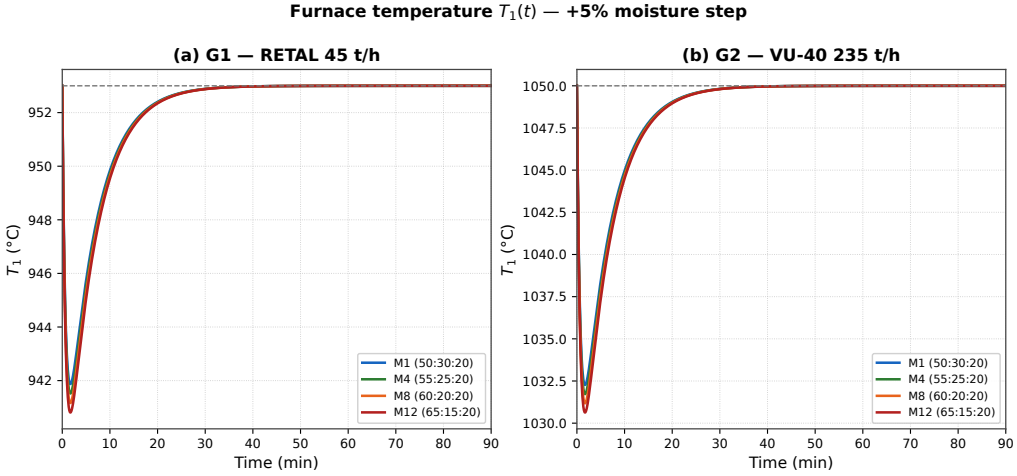


Figure 1. Temporal evolution of furnace temperature (T_1) under +5% step perturbation in fuel moisture for four representative mixtures.

Results reveal furnace temperature drops rapidly during the first 5 min post-perturbation, reaching $\Delta T_{1,\max}$ values between 11.14 °C (M1, G1) and 12.20 °C (M12, G1) in the RETAL generator, and between 17.76 °C (M1, G2) and 19.39 °C (M12, G2) in the VU-40. Greater drop magnitude in G2 is explained by its higher combustion energy to furnace thermal mass ratio (Q_{comb}/M_1). Mixtures with higher moisture (M8, M12) consistently show greater drops than lower-moisture mixtures (M1, M4), confirming effective ternary mixture moisture as the determining factor of combustion zone perturbation magnitude. Node 1 recovery time is on the order of 15–20 min, governed by fuel flow controller response speed ($\tau \approx 5.5$ min).

3.1.2. Transient Response of Node 2 (Water/Steam System)

Steam temperature (T_2) constitutes the model's operationally relevant variable, as it determines steam quality delivered to sugar processing or turbogenerator. Unlike T_1, T_2 response is mediated by two coupling mechanisms (radiation and convection) and damped by the high thermal mass of the water/steam system. Figure 2 presents T_2 evolution for the same mixtures and generators.

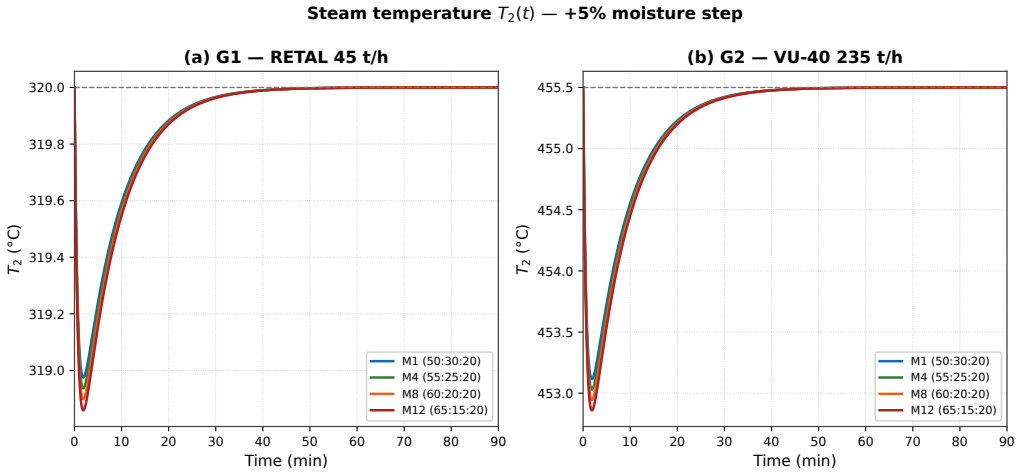


Figure 2. Temporal evolution of steam temperature (T_2) under +5% step moisture perturbation for four representative mixtures.

The maximum deviation of steam temperature is significantly lower than the deviation of furnace temperature: $\Delta T_{2,\max}$ ranges between 1.03 °C (M1, G1) and 1.14 °C (M12, G1) in the RETAL generator, and between 2.39 °C (M1, G2) and 2.65 °C (M12, G2) in the VU-40. The attenuation ratio $(\Delta T_{1,\max}/\Delta T_{2,\max})$ clusters by technology, at ≈10.9 for G1 and ≈7.4 for G2, demonstrating that the high thermal mass of the water/steam system acts as an effective thermal filter, absorbing most of the disturbance generated in the combustion zone. The temporal trajectories of T_2 show an initial drop followed by a damped recovery toward the nominal value, behavior consistent with the action of the fuel flow controller and the thermal inertia of Node 2. Consequently, the comparative dynamic stability between mixtures is evaluated using $\Delta T_{2,\max}$, since this quantity directly and consistently represents the amplitude of the disturbance transmitted to the steam side under a step change of +5% in fuel moisture. For the reference mixture M1, the steam-side response was further verified under symmetric ±5% moisture steps and under ±10% steam-load and ±10% excess-air steps (Supplementary Material, Figures S1–S3). The moisture perturbation recovers toward the nominal value once the fuel-flow controller compensates, whereas the steam-load and excess-air steps settle at a shifted operating point; in all cases the steam temperature deviation remains within a few degrees, confirming the robustness of the inter-node attenuation beyond the moisture perturbation.

3.1.3. Maximum Deviation Comparison Among 12 Mixtures

To establish quantitative comparison among all evaluated ternary formulations, maximum temperature deviations at each node for the 12 mixtures and both generators are presented in Figure 3.

Monotonic increase of $\Delta T_{1,\max}$ with mixture moisture is observed in both generators. G2 presents systematically higher values than G1 (factor ≈ 1.6×), reflecting greater combustion sensitivity to LHV variations. Difference between lowest-moisture mixture (M1, $W = 35.5\%$) and highest-moisture mixture (M12, $W = 40.75\%$) is 1.06 °C in G1 and 1.63 °C in G2.

Steam deviation (Figure 4) follows same monotonic trend as furnace but with significantly lower amplitudes and 2.3× technological differentiation factor. All deviations remain below 3 °C, within acceptable operating margin for industrial steam generators. G2 proves more sensitive in both furnace and steam, indicating high-pressure technologies require stricter fuel quality control when operating with ternary biomass mixtures.

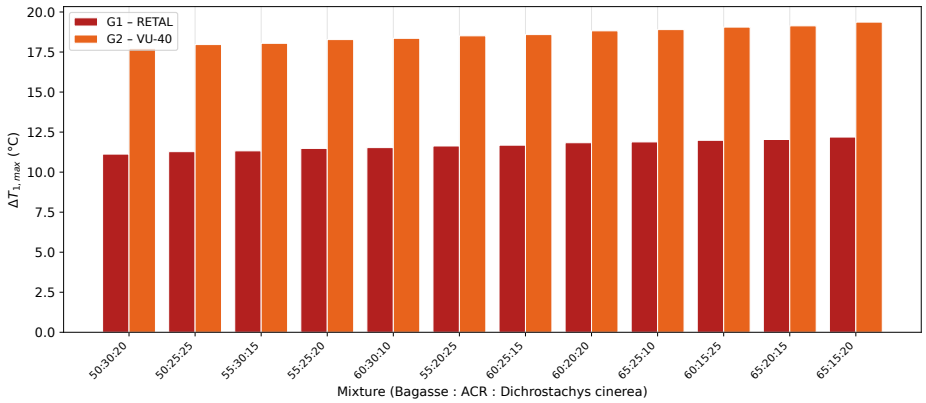


Figure 3. Maximum furnace temperature deviation ($\Delta T_{1,\max}$) for 12 evaluated ternary mixtures in both generators.

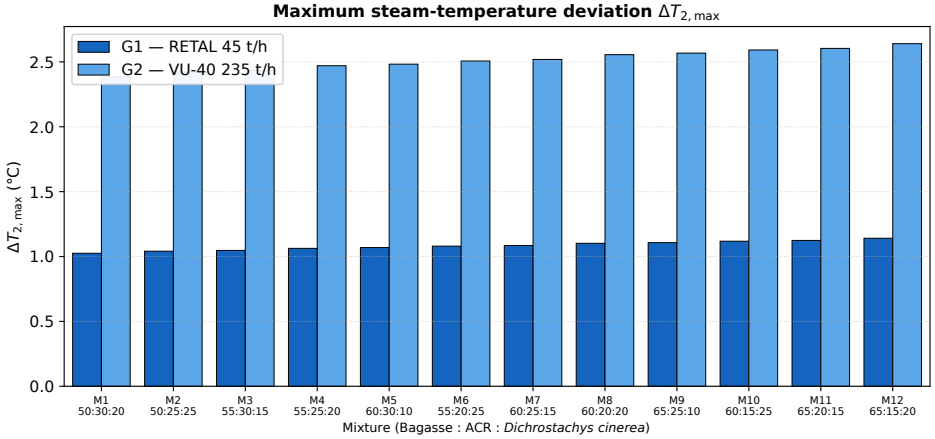


Figure 4. Maximum steam temperature deviation ($\Delta T_{2,\max}$) for 12 evaluated ternary mixtures in both generators.

3.2. Statistical Analysis of the Dynamic Model

3.2.1. Linear Regression: Maximum Deviation vs. Mixture Moisture

To quantify the functional dependence between mixture moisture and system dynamic response, simple linear regression analysis was performed between $\Delta T_{1,\max}$ (Figure 5) and $\Delta T_{2,\max}$ (Figure 6) and effective mixture moisture W.

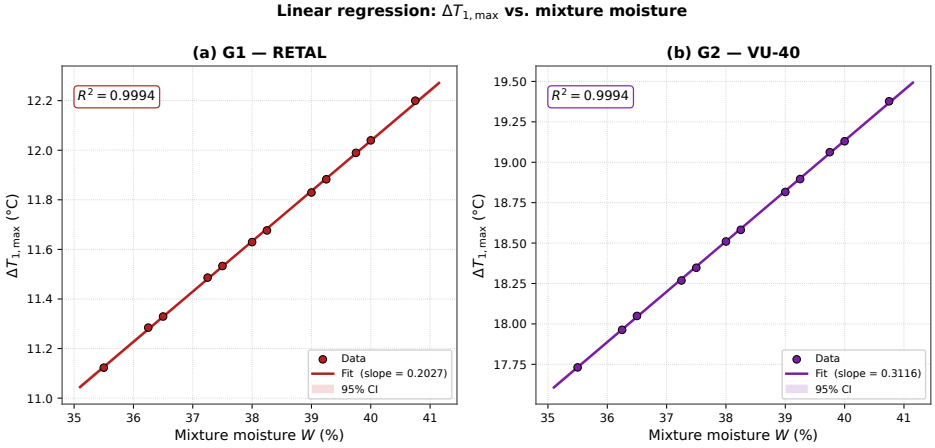


Figure 5. Linear regression of $\Delta T_{1,\max}$ against mixture moisture, with 95% confidence band.

Obtained coefficients of determination ($R^2 = 0.9994$ for both generators) confirm mixture moisture explains 99.94% of $\Delta T_{1,\max}$ variability within evaluated compositional window. Slope is 0.2027 °C/% for G1 and 0.3116 °C/% for G2, quantifying that each percentage point moisture increase produces additional furnace temperature drop of 0.20 °C (G1) or 0.31 °C (G2). Slope ratio (G2/G1 = 1.54) reflects greater thermal sensitivity of high-pressure generator combustion zone.

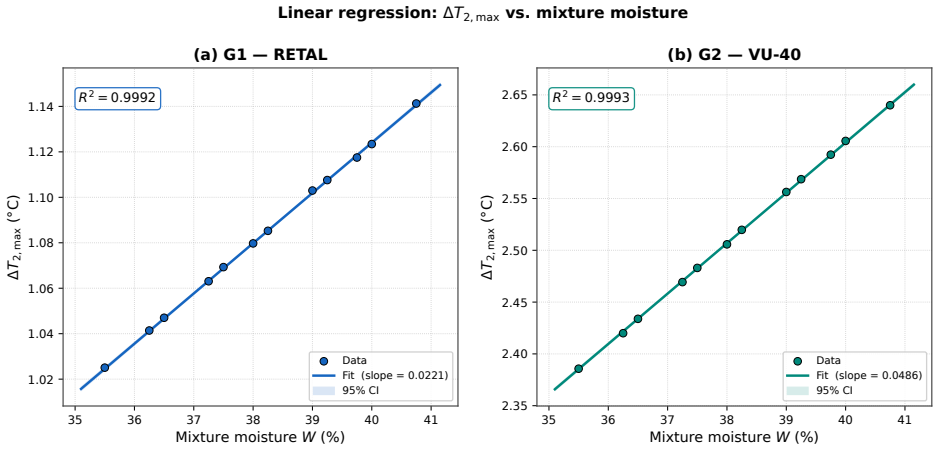


Figure 6. Linear regression of $\Delta T_{2,\max}$ against mixture moisture, with 95% confidence band.

Node 2 correlation is equally high ($R^2 = 0.9992$ for G1, $R^2 = 0.9993$ for G2), with slopes of 0.0221 °C/% (G1) and 0.0486 °C/% (G2). Node 2 slope ratio (G2/G1 = 2.20) exceeds Node 1 ratio, indicating water/steam mass damping effect is not proportional between technologies: G2, despite greater absolute M_2 (142,000 vs. 32,000 kg), exhibits lower M_2/Q_{useful} ratio, reducing relative perturbation absorption capacity.

3.2.2. OAT Sensitivity Analysis (One-at-a-Time, ±10%)

OAT sensitivity analysis evaluates effect of individual ±10% variations in each model parameter on response variable $\Delta T_{2,\max}$, holding other parameters constant (Table 9). This approach identifies parameters exerting greatest influence on model prediction (Figure 7).

Table 9. OAT sensitivity analysis results (±10%). Reference case: M1 (50:30:20), G1 RETAL.

Parameter	$\Delta T_{2,\max}$ (−10%)	$\Delta T_{2,\max}$ (Ref)	$\Delta T_{2,\max}$ (+10%)	Sensitivity (%)
τ (controller)	0.912	1.025	1.138	22.1
M_2 (water/steam mass)	1.138	1.025	0.932	20.1
ε (flame emissivity)	0.933	1.025	1.117	17.9
UA (convective)	1.005	1.025	1.045	3.9
M_1 (furnace mass)	1.034	1.025	1.015	1.9
C_{p1} (furnace spec. heat)	1.034	1.025	1.015	1.9

Three most influential parameters are controller time constant τ (22.1%), water/steam system thermal mass M_2 (20.1%), and flame emissivity ε (17.9%), jointly representing 60.1% of total sensitivity. Conversely, Node 1 exclusive parameters (M_1 and C_{p1}) contribute only 1.9% each to $\Delta T_{2,\max}$ variability. This result carries significant methodological implication: uncertainty in furnace parameter estimation does not significantly compromise model predictive capacity for the operationally relevant variable (T_2).

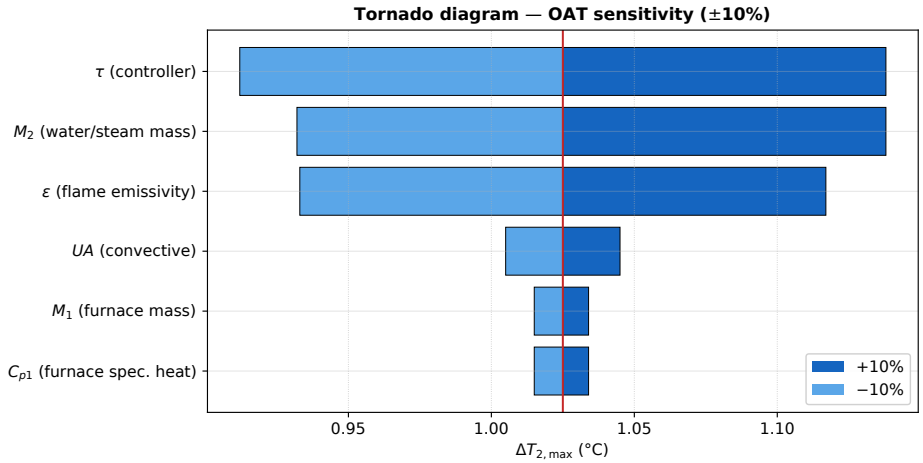


Figure 7. Tornado diagram of parametric influence on $\Delta T_{2,\max}$ (OAT $\pm$ 10%).

3.2.3. Monte Carlo Uncertainty Analysis

While OAT sensitivity evaluates individual parameter effects independently, Monte Carlo simulation with $N = 2000$ runs quantifies the combined effect of simultaneous parameter uncertainty (Table 10). The full dynamic model is executed within each iteration, propagating the uncertainty of the three parameters identified by the OAT screening as the most influential on the steam-side response—the controller time constant ($\tau \in [4, 7]$ min, nominal $\tau = 5.5$ min), the thermal mass of the water/steam system (M_2, $\pm$10% about its nominal value), and the flame emissivity ($\varepsilon \in [0.40, 0.50]$, nominal $\varepsilon = 0.45$)—all sampled from independent uniform distributions and with ranges grounded in physical criteria and in the literature for industrial biomass combustion (Figure 8). The damping factor remains robust under this uncertainty, with a median of $F = 10.9$ (90% CI: 10.0–11.7) for G1 and $F = 7.4$ (90% CI: 6.8–8.1) for G2 (Figure S4), consistent with the technology-clustered attenuation ($\approx$10.9 for G1 and $\approx$7.4 for G2) obtained across the twelve mixtures and confirming that the relative conclusions do not depend on the point values of these parameters.

Table 10. Monte Carlo analysis results ($N = 2000$). Case: M1 (50:30:20), G1 RETAL.

Statistic	$\Delta T_{1,\max}$ (°C)	$\Delta T_{2,\max}$ (°C)
Mean	11.07	1.035
Standard deviation	1.39	0.274
90% CI	[8.78, 13.36]	[0.58, 1.49]
Coefficient of variation	12.6%	26.5%

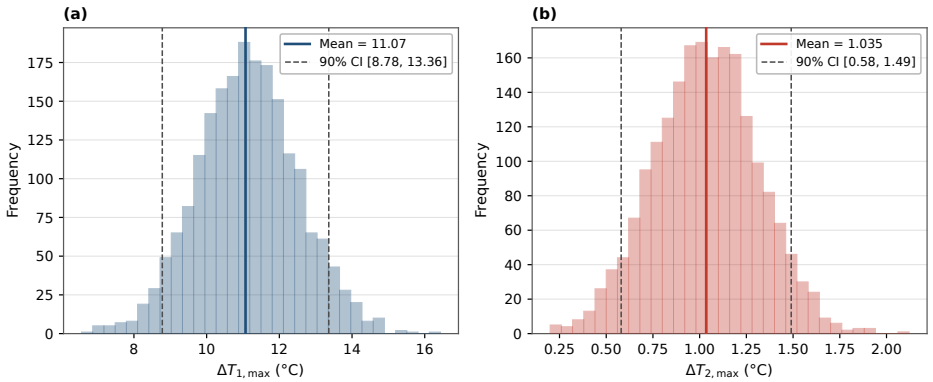


Figure 8. Probability distributions from Monte Carlo analysis. (**a**) $\Delta T_{1,\max}$ (Node 1–furnace); (**b**) $\Delta T_{2,\max}$ (Node 2–steam).

Results show $\Delta T_{2,\max}$ distributes with 90% confidence interval [0.58, 1.49] °C, confirming steam temperature deviation remains below 2 °C even under combined parametric uncertainty conditions.

3.3. Connection of Dynamic Model with Other Integrated Framework Models

The dynamic model does not operate in isolation within the proposed methodological framework. Its outputs directly feed other models, establishing a causal chain linking transient behavior with steady-state performance (Models 1 and 2) and environmental sustainability (Model 4). Figure 9 illustrates this connection for representative case M1 (50:30:20) in G1 RETAL generator.

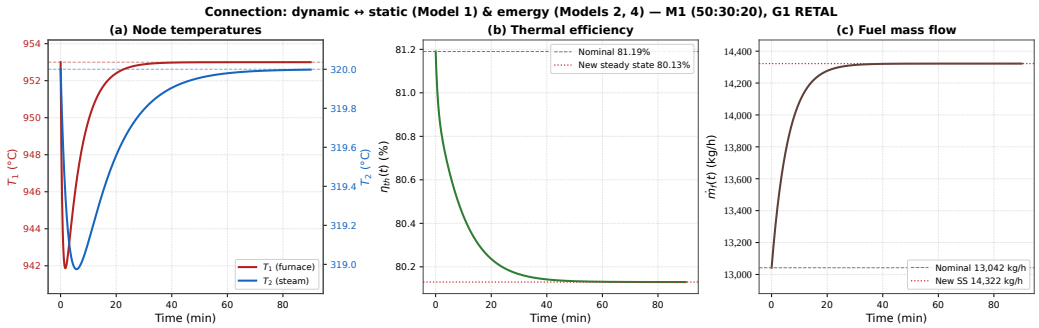


Figure 9. Connection between dynamic model and other integrated framework models for M1 (50:30:20), G1 RETAL. (**a**) Temperatures T_1 and T_2 (Equations (4)–(6)); (**b**) Instantaneous thermal efficiency $\eta_{th}(t)$—connection with Model 1; (**c**) Fuel mass flow $\dot{m}_f(t)$—connection with Models 2 (exergy) and 4 (emergy).

Panel (a) shows both nodes evolution: rapid T_1 drop and damped T_2 response. Panel (b) presents instantaneous thermal efficiency $\eta_{th}(t) = Q_{\text{useful}}/Q_{\text{comb}}(t)$, dropping during transient from the nominal 81.19% value (Table 7) and recovering as controller adjusts fuel flow. At steady state ($t \to \infty$), $\eta_{th}(t)$ exactly converges to value predicted by static model under perturbed conditions, constituting internal consistency verification. Panel (c) shows fuel flow $\dot{m}_f(t)$, gradually increasing from 13,042 kg/h to 14,322 kg/h (ratio $\dot{m}_f^*/\dot{m}_f = 1.098$). This 9.8% fuel consumption increase propagates directly to Model 2 and Model 4.

3.4. Emergy Model

3.4.1. Emergy Calculation Procedure

Emergy evaluation quantifies solar emergy embodied in all matter, energy, and service flows required to sustain the steam generation process, expressing them in a common unit (solar emjoule, seJ). The procedure followed principles established by Odum (1996) [38] and Brown & Ulgiati (2004) [39], using transformities reported by Jiménez Borges et al. [47] for the Cuban sugar context.

For each mixture–generator combination, the calculation follows the sequence: (1) determine the required fuel mass flow from thermal efficiency and mixture LHV; (2) decompose the total flow into bagasse, ACR, and *Dichrostachys cinerea* mass fractions per mixture composition; (3) annualize all flows multiplying by 3600 h/year (150-day harvest); (4) calculate the emergy of each flow multiplying quantity by the corresponding transformity; (5) classify flows as renewable (R), non-renewable (N), and economic (F = M + S, i.e., purchased materials M and services S); (6) calculate the emergy indicators: $EYR = U/F$, $ELR = (N + F)/R$, $ESI = EYR/ELR$, $\%R = R/U \times 100$.

3.4.2. Flow Classification

Flows were classified as follows. As renewable (R): combustion air, bagasse, ACR (cane harvest residues, annual cycle), and *Dichrostachys cinerea* (invasive species with regeneration capacity). As non-renewable (N): generator feedwater. As economic flows (F = M + S): as purchased materials (M), bagasse transport costs, ACR collection and transport, *Dichrostachys cinerea* acquisition, and water cost; as purchased services (S), equipment maintenance and human labor.

3.5. Adopted Transformities

The transformities adopted for the emergy assessment are summarized in Table 11. These values were taken from Jiménez Borges et al. [47] and are used to convert the different material, energy, and economic flows into a common emergy basis.

Table 11. Adopted transformities for emergy model [47].

Flow	Transformity	Unit	Classification
Bagasse	9.5501×10^9	seJ/kg	R
ACR	3.2667×10^9	seJ/kg	R
Dichrostachys cinerea	7.5773×10^6	seJ/J	R
Combustion air	9.82×10^2	seJ/J	R
Feedwater	5.4264×10^5	seJ/kg	N
Emergy/money ratio	4.60×10^{12}	seJ/$	M, S
Human labor	3.93×10^6	seJ/J	S

3.6. Emergy Model Results

3.6.1. Emergy Sustainability Index (ESI)

The emergy sustainability index (ESI, Figure 10) serves as integrating indicator of the emergy model. ESI values > 5 indicate long-term sustainable systems, while values < 1 suggest high dependence on non-renewable or imported resources. The resulting ESI ranking of the twelve mixtures is preserved under a $\pm 30\%$ perturbation of the biomass transformities, propagated through the emergy model by Monte Carlo simulation (Supplementary Material, Figure S5), indicating that the relative sustainability ordering is not an artifact of the specific transformity values adopted.

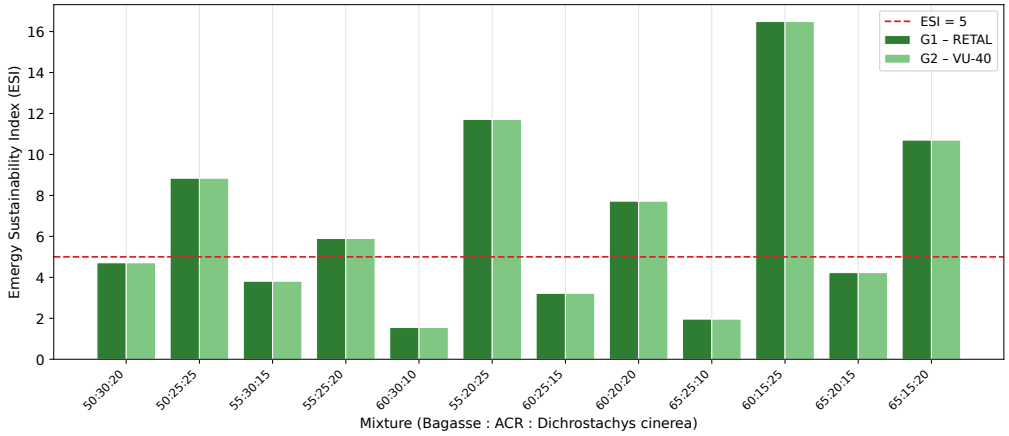


Figure 10. Emergy sustainability index (ESI) for 12 ternary mixtures in both generators. Dashed line: ESI = 5 threshold.

Results show marked differentiation between mixtures, with ESI varying from 1.55 (M5, 60:30:10) to 16.49 (M10, 60:15:25). Six mixtures exceed the long-term sustainabil-

ity threshold (ESI > 5): M10 (16.49), M6 (11.71), M12 (10.70), M2 (8.84), M8 (7.72), and M4 (5.90). Mixtures with 30% ACR (M1, M3, M5) consistently show lowest ESI values, penalized by high ACR collection and transport cost (7.53 $/kg). Generator differences are negligible (<0.01 in ESI), confirming emergy sustainability depends on fuel composition, not conversion technology.

3.6.2. Renewability Ratio (%R)

%R (Figure 11) varies from 45.66% (M5) to 78.22% (M10). Values are consistent with those reported by Jiménez Borges et al. [47] for binary variants (%R = 23.58–58.04% in RETAL), but higher on average, explained by *Dichrostachys cinerea* inclusion as low-cost third renewable component. Mixtures with higher *Dichrostachys cinerea* proportion (≥20%) and lower ACR proportion (≤20%) maximize renewability.

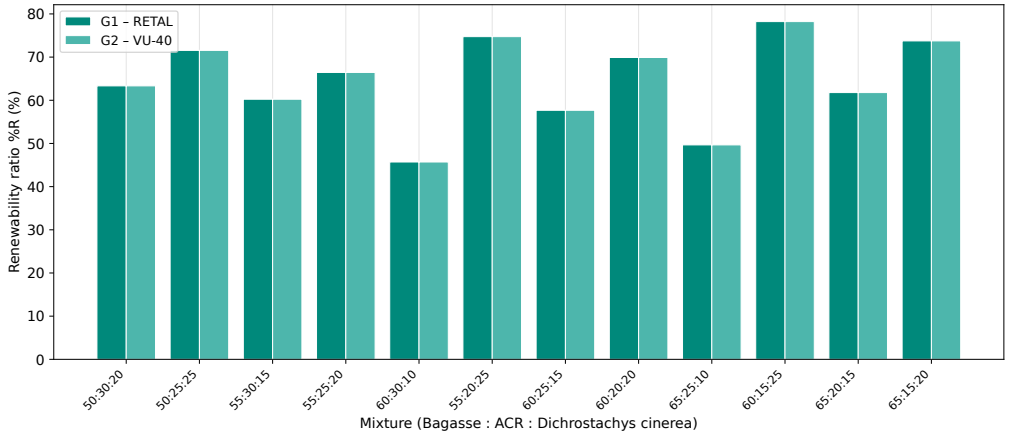


Figure 11. Renewability ratio (%R) for 12 ternary mixtures in both generators.

3.6.3. Emergy Yield Ratio (EYR)

EYR (Figure 12) varies from 1.84 (M5) to 4.59 (M10). EYR values near 1 (M5 = 1.84, M9 = 1.96) indicate system functions primarily as economic input transformer. Conversely, M10 (EYR = 4.59) and M6 (EYR = 3.96) demonstrate substantial economic resource amplification capacity. The EYR determining variable is F magnitude (economic emergy), dominated by ACR collection cost.

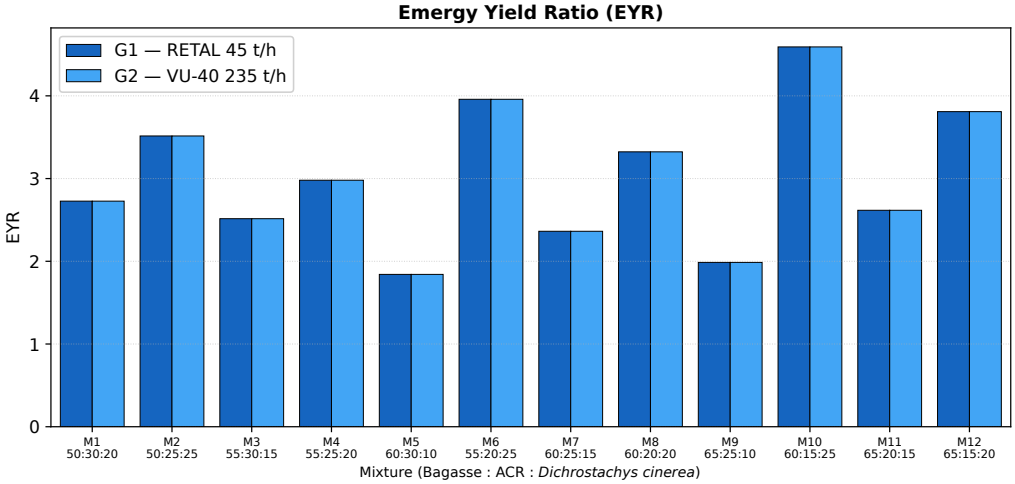


Figure 12. Emergy yield ratio (EYR) for 12 ternary mixtures in both generators.

3.6.4. Environmental Loading Ratio (ELR)

ELR (Figure 13) varies from 0.28 (M10) to 1.19 (M5). All evaluated mixtures exhibit ELR < 2, classifying the system as low environmental impact per Brown & Ulgiati (2004) [39] scale. High-ACR mixtures (M5, M9) approach ELR = 1, indicating ACR increase not only penalizes economic efficiency but also deteriorates the process environmental profile.

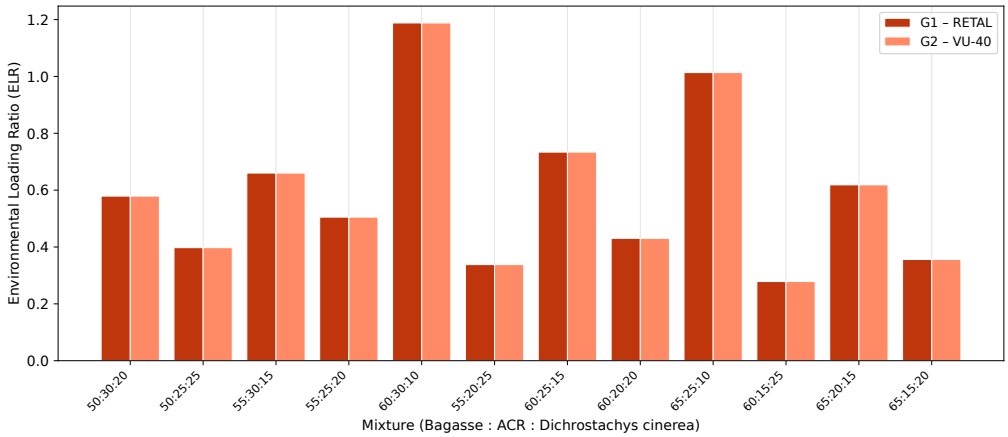


Figure 13. Environmental loading ratio (ELR) for 12 ternary mixtures in both generators.

3.7. Multidimensional Integration: Central Finding

The fundamental purpose of the integrated framework is to evaluate whether the optima identified by each individual model converge toward the same mixture or point to different formulations. Figure 14 presents direct comparison of four models for four representative mixtures.

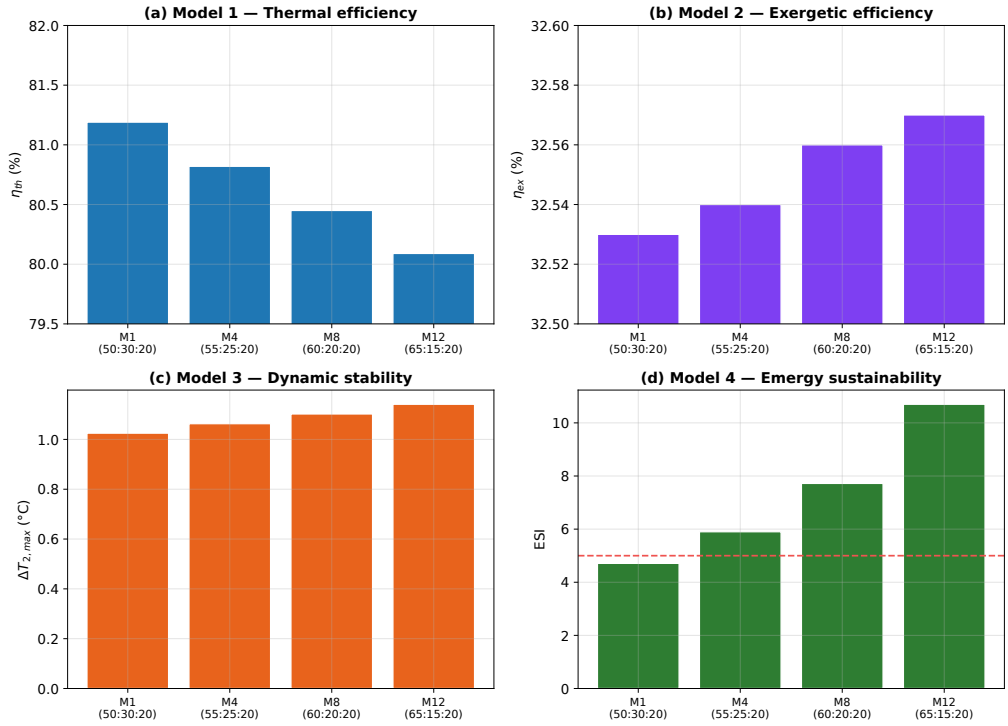


Figure 14. Absolute performance comparison of four representative ternary mixtures in G1 (RETAL). (**a**) Indirect thermal efficiency (η_{th}); (**b**) exergy efficiency (η_{ex}); (**c**) dynamic stability expressed as maximum steam temperature deviation ($\Delta T_{2,\max}$); and (**d**) emergy sustainability index (ESI).

Figure 14 conclusively demonstrates that the optima of each dimension do not coincide. In panel (a), thermal efficiency reaches its maximum at M1 (50:30:20; $W = 35.5\%$). In panel (b), exergy efficiency exhibits much smaller variations and reaches its highest value at M12 (65:15:20; $W = 40.75\%$), although the difference relative to M10 is marginal. In panel (c), dynamic stability, inversely assessed through $\Delta T_{2,\max}$, is highest in M1. In panel (d), emergy sustainability (ESI) reaches its highest value at M10 (60:15:25; ESI = 16.49) within the complete set of 12 mixtures; since M10 does not belong to the subset of four mixtures represented in this figure, within that subset the mixture with the highest ESI is M12 (ESI = 10.70). This result confirms that emergy sustainability is governed primarily by system-level resource use and environmental support. The ordinal rankings of the 12 mixtures across the four dimensions are summarized in Table 12 and visualized as a heat map in Figure 15.

Table 12. Multidimensional ranking of the 12 ternary mixtures across thermal efficiency ($\eta_{th,avg}$), exergy efficiency ($\eta_{ex,avg}$), dynamic stability ($\Delta T_{2,\max}$, G1), and emergy sustainability (ESI). Rank 1 indicates the best performance.

Mix	W (%)	$\eta_{th,avg}$	Rank	$\eta_{ex,avg}$	Rank	$\Delta T_{2,\max}$	Rank	ESI	Rank
M1	35.50	83.84	1	35.96	10	1.025	1	4.71	7
M2	36.25	83.73	2	35.97	7	1.041	2	8.84	4
M3	36.50	83.63	3	35.96	11	1.047	3	3.81	9
M4	37.25	83.52	4	35.97	8	1.063	4	5.90	6
M5	37.50	83.42	5	35.96	12	1.069	5	1.55	12
M6	38.00	83.40	6	35.98	5	1.080	6	11.71	2
M7	38.25	83.31	7	35.97	9	1.085	7	3.22	10
M8	39.00	83.19	8	35.99	3	1.102	8	7.72	5
M9	39.25	83.09	9	35.98	6	1.107	9	1.96	11
M10	39.75	83.08	10	36.00	1	1.118	10	16.49	1
M11	40.00	82.98	11	35.99	4	1.124	11	4.23	8
M12	40.75	82.87	12	36.00	2	1.141	12	10.70	3

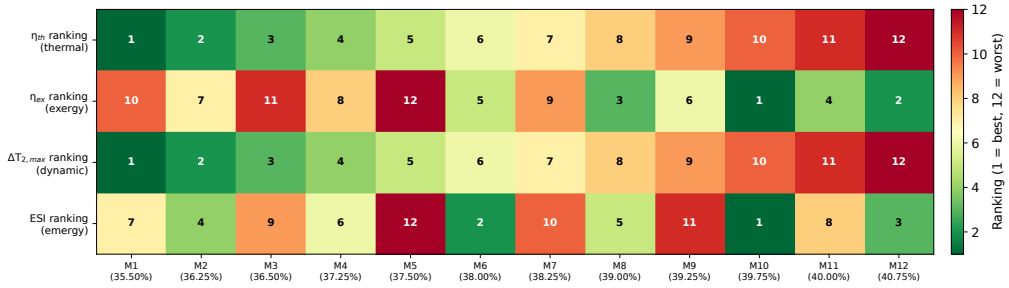


Figure 15. Integrated ranking-based comparison of the complete set of 12 ternary mixtures in G1 (RETAL). Heat map of ordinal ranking for thermal efficiency, exergy efficiency, dynamic stability, and emergy sustainability. Ranking values range from 1 (best) to 12 (worst).

4. Discussion

4.1. Indirect Thermal Efficiency and Moisture Dominance

The indirect thermal efficiencies obtained (80.09–81.19% for G1 RETAL at 1.9 MPa; 85.65–86.49% for G2 VU-40 at 6.2 MPa) position within the upper range reported for bagasse boilers. Cortes-Rodríguez et al. [7] experimentally evaluated six water-tube boilers in São Paulo sugar mills per ASME PTC 4-2008, obtaining efficiencies of 70–84% with flue gas losses of 17–18% as dominant factor. Present study values exceed that Brazilian sample average due to lower flue gas outlet temperatures (213.7 °C in G1, 179.4 °C in G2). Sosa-

Arnao and Nebra [8] reported first-principle efficiencies of 82–84% for 40–60 bar boilers, values consistent with present G2 results.

The mechanism by which moisture dominates simultaneously the thermal, exergetic, and transient dimensions is rooted in a single, prior variable: the wet-basis lower heating value. An increase in moisture reduces LHV_{wet} through two cumulative effects—it lowers the combustible mass fraction and adds the latent heat required to evaporate the contained water—and this reduction propagates coherently to each analysis. In the thermal dimension, a lower LHV_{wet} requires higher fuel flow and raises hot-gas losses (q_2), reducing efficiency. In the exergetic dimension, the same LHV decrease lowers the specific input exergy of the fuel (Supplementary Material, Equation (S2)). In the transient dimension, moisture modifies the combustion heat input and therefore the magnitude of the thermal perturbation the system must damp. The three responses thus share a common physicochemical root. This dominance is qualitatively universal for biomass combustion (the LHV_{wet} mechanism is general), whereas its quantitative magnitude is technology-specific, as evidenced by the different moisture sensitivities of RETAL and VU-40.

Moisture sensitivity $d\eta_{th}/dW = -0.212$ pp/% (G1) and -0.161 pp/% (G2) aligns with the empirical rule documented by Mo et al. [9] and Kabeyi and Olanrewaju [6]. However, present results refine this generic relationship: 2.12 pp/10% in RETAL and only 1.61 pp/10% in VU-40, confirming high-pressure generators exhibit lower sensitivity to fuel variability. The specific contribution of this work demonstrates $R^2 > 0.99$ holds for 12 ternary formulations of three distinct biomasses, filling a gap in a literature dominated by binary biomass-coal blends [48,49].

4.2. Exergy Efficiency and Its Decoupling from Thermal Efficiency

Exergy efficiencies of 32.53–32.57% (G1) and 39.38–39.43% (G2) position in the literature medium-high range. Cavalcanti et al. [50] obtained $\eta_{ex} = 16.89\%$ for a sugarcane bagasse cogeneration system, and Lythcke-Jørgensen et al. [51] reported $\eta_{ex} = 21.07\%$ for a combined heat and power configuration. Present study superior values (32.5–39.4%) attribute to higher steam parameters and lower ternary mixture moisture. Molina et al. [22], genetically optimizing a 34 MW Colombian bagasse boiler, improved exergy efficiency from 27.8% to 29.1%; the present 32.5% for a similar RETAL exceeds that optimized value.

Across the evaluated compositional window ($W = 35.5$–40.75%), the average exergy efficiency spans only 0.04 percentage points (35.96–36.00%), a range comparable to the measurement uncertainty of industrial boiler instrumentation (± 0.5 pp). Exergy efficiency is therefore effectively invariant with respect to blend composition, and the relevant discrimination among mixtures arises in the thermal, dynamic, and emergy dimensions rather than in the exergy dimension. This invariance has a clear thermodynamic basis: thermal efficiency is governed by quantitative losses (q_2, controlled by W), whereas exergy efficiency is governed by the lower heating value and the elemental composition of the fuel, whose sensitivity to moisture is more than an order of magnitude lower. The negative Pearson correlation between η_{th} and η_{ex} ($r = -0.850$) reflects this differing sensitivity rather than a competing design objective: because η_{ex} is essentially constant, mixture selection is driven by thermal performance, dynamic stability, and emergy sustainability.

It should be noted that the present exergy treatment quantifies the overall exergy efficiency but does not spatially resolve the exergy destruction among the combustion chamber, the heat-transfer surfaces, and the stack. A spatially resolved, component-level exergy decomposition—separating combustion irreversibility from heat-transfer irreversibility along the lines of Tsatsaronis and Park [28]—is identified as a relevant direction for future work, as it would localize the avoidable exergy destruction and complement the integrated assessment developed here.

4.3. Two-Node Dynamic Model: Confrontation with the Literature

The two-node transient formulation occupies a deliberate intermediate position between lumped single-node balances and spatially resolved CFD models. Mameri et al. [32] developed a 0D Bond-Graph model for a 30 kW pellet boiler and identified radiation as the dominant transfer mechanism (97.6% of the total), a conclusion consistent with the radiative coupling that governs Node 1 in the present model. Gómez et al. [33] and Atsonios et al. [34] achieved spatial resolution through CFD and 1D process models, respectively, at a computational cost that precludes the systematic screening of 12 mixtures across two technologies performed here. The present model reproduces the qualitative transient behavior reported by Carlon et al. [36]—a rapid combustion-side response followed by a damped working-fluid response—while remaining tractable enough for compositional screening. Its principal limitation, shared with all the cited lumped formulations, is the omission of drum-pressure dynamics; the model is therefore restricted to temperature transients under moderate moisture perturbations and is not intended to capture pressure-driven safety transients.

4.4. Emergy Sustainability: Contrast with Global Bioenergy Systems

The renewability percentages obtained (%R = 45.66–78.22%) and the ESI range (1.55–16.49) are consistent with, and on average more favorable than, the binary-mixture values reported by Jiménez Borges et al. [47] for the same Cuban sugar context (%R = 23.58–58.04% in RETAL). The improvement is attributable to the inclusion of *Dichrostachys cinerea* as a low-cost third renewable component. Relative to global bioenergy emergy studies—Edrisi et al. [52] for marginal-land bioenergy in India and Ren et al. [53] for power-generation systems—the present systems exhibit comparatively low environmental loading (ELR < 2 for all mixtures), reflecting the predominantly renewable input structure. The dominant penalty on sustainability is the economic emergy (F), concentrated in the ACR collection and transport cost; mixtures with high ACR fractions (M5, M9) consequently exhibit the lowest ESI, while mixtures favoring *Dichrostachys cinerea* (M10, M6, M12) achieve the highest.

4.5. Statistical Independence Between Dimensions: Central Finding

The most consequential outcome of the integrated assessment is that the optima of the four dimensions do not coincide. Thermal efficiency and dynamic stability both rank M1 first, since both are governed by moisture, but emergy sustainability ranks M10 first and exergy efficiency ranks M10/M12 first. The Spearman rank correlation between thermal efficiency and emergy sustainability is $\rho = -0.182$ ($p = 0.572$, $n = 12$), statistically indistinguishable from zero, indicating that thermal and emergy rankings are effectively independent within the evaluated compositional space. A criterion that optimizes a single dimension is therefore insufficient: optimizing thermal efficiency (M1) sacrifices emergy sustainability (ESI = 4.71, rank 7 of 12), whereas optimizing emergy sustainability (M10) sacrifices thermal efficiency (rank 10 of 12). Compromise mixtures such as M2 and M4—which combine high thermal ranks (2 and 4) with above-threshold emergy sustainability (ESI = 8.84 and 5.90)—emerge only when the dimensions are considered jointly, which is precisely the value added by the integrated framework over partial approaches.

4.6. Optimal Compositional Zone and Transferability

Considered jointly, the results delimit a compromise compositional zone of approximately 50–55% bagasse, 25–30% ACR, and 20–25% *Dichrostachys cinerea* (mixtures M2 and M4), within which thermal efficiency remains near its maximum, dynamic deviations stay below the operational margin, and emergy sustainability exceeds the long-term thresh-

old (ESI > 5). It must be emphasised that the dynamic and emergy results are model predictions verified for internal consistency—through the exact convergence of the transient steady state to the static prediction and the analytical reproduction of the emergy indicators—rather than validated against transient plant measurements, in the sense of Sargent [45]. Consequently, while the methodological framework is transferable to other biomass combustion contexts, the specific compositional zone, transformities, and sensitivity coefficients are conditioned by the Cuban sugar-industry setting and the biomass types evaluated, and should be re-estimated for other regions and feedstocks.

4.7. Emissions and Economic Implications

Although the present study does not develop a dedicated emissions inventory, the emergy framework partially captures the environmental dimension through the environmental loading ratio, and the low ELR values (<2) indicate a limited environmental burden per unit of useful steam. The economic dimension is likewise embedded in the emergy economic flow (F), dominated by the ACR collection and transport cost (7.53 \$/kg), which is the principal lever on both EYR and ESI. A full life-cycle emissions assessment and a dedicated techno-economic analysis—including capital and operating expenditure and a levelised cost of steam—are identified as complementary studies that would strengthen the practical applicability of the framework, in line with the reviewers' suggestions.

4.8. Recommendations

Three practical recommendations follow from the results. First, for operators prioritising thermal performance and dynamic stability, low-moisture mixtures in the M1–M4 range are preferred, subject to ACR availability. Second, for operators prioritising long-term sustainability, mixtures favouring *Dichrostachys cinerea* (M6, M10, M12) maximise renewability and the emergy sustainability index. Third, where a single robust setpoint is required, the compromise zone (M2, M4) offers the best simultaneous balance across the four dimensions and is therefore recommended as the default operating window. In all cases, effective mixture moisture should be monitored and controlled as the dominant structural variable, since it governs thermal efficiency, dynamic response, and fuel consumption simultaneously.

4.9. Study Limitations

This study is subject to several limitations. First, the dynamic results are model predictions verified for internal consistency but not validated against transient measurements from the operating boilers. Second, the two-node model omits drum-pressure dynamics, combustion kinetics, and drying dynamics, and is therefore restricted to temperature transients under moderate moisture perturbations. Third, the Monte Carlo parameter ranges are engineering estimates of parameter uncertainty in the absence of plant-specific calibration data. Fourth, the emergy transformities and economic costs are drawn from the Cuban sugar context and are not directly transferable to other regions. Fifth, the exergy analysis quantifies the overall efficiency without spatially resolving exergy destruction among components. These limitations delimit the scope of the conclusions and define the priorities for future work.

5. Conclusions

An integrated methodological framework combining static energy, exergy, two-node transient dynamic, and emergy models was developed and applied to twelve ternary mixtures of sugarcane bagasse, agricultural crop residues, and *Dichrostachys cinerea* in two steam-generator technologies. The framework moves beyond isolated efficiency assess-

ment toward a holistic characterization of biomass boiler performance under technically plausible ternary mixtures.

The effective moisture content of the mixture was identified as the dominant structural control variable, governing simultaneously the wet-basis lower heating value, the specific fuel consumption, the principal thermal loss, the indirect thermal efficiency, and the dynamic stability of the system, with coefficients of determination above 0.99 for the transient deviations. The two-node dynamic model revealed a technology-dependent inter-node thermal damping factor (≈10.9 for the RETAL and ≈7.4 for the VU-40 generator) between the combustion zone and the water/steam system, keeping steam temperature deviations below 3 °C under +5% moisture perturbations, and the sensitivity analysis identified the controller time constant, the thermal mass of the water/steam system, and the flame emissivity as the most influential parameters.

The central finding is that the optima of the four dimensions do not coincide: thermal efficiency and dynamic stability favour low-moisture mixtures (M1), whereas emergy sustainability favours mixtures rich in *Dichrostachys cinerea* (M10), with thermal and emergy rankings statistically independent. A compromise compositional zone of approximately 50–55% bagasse, 25–30% ACR, and 20–25% *Dichrostachys cinerea* (mixtures M2 and M4) provides the best simultaneous balance across the four dimensions and is recommended as the default operating window.

While the methodological framework is transferable to other biomass combustion contexts, the numerical results—optimal compositional zones, emergy indicators, and dynamic sensitivity coefficients—are specific to the Cuban sugar-industry conditions, the adopted transformities, and the biomass types evaluated. Future work should address transient validation against plant measurements, the incorporation of drum-pressure dynamics, a spatially resolved exergy decomposition, a life-cycle emissions inventory, and a dedicated techno-economic analysis.

Supplementary Materials: The following supporting information can be downloaded at: https://www.mdpi.com/article/10.3390/biomass6030046/s1, Figure S1: Symmetric transient response of the furnace temperature (T_1) and the steam temperature (T_2) to ±5% moisture steps for blend M1 (50:30:20), computed with the two-node model. (a,b) furnace temperature T_1; (c,d) steam temperature T_2; left column G1 (RETAL 45 t/h), right column G2 (VU-40 235 t/h). Dotted lines indicate the nominal values; Figure S2: Steam temperature (T_2) response to ±10% steps in the boiler-outlet excess-air coefficient (α_{gsal}: 2.0 → 1.8 and 2.2) for blend M1 (50:30:20), with the hot-gas loss q_2 recalculated through the static model at each perturbed value. (a) G1 (RETAL 45 t/h); (b) G2 (VU-40 235 t/h). Dotted lines indicate the nominal values; Figure S3: Steam temperature (T_2) response to ±10% steps in the boiler-outlet excess-air coefficient (α_{gsal}: 2.0 → 1.8 and 2.2) for blend M1 (50:30:20), with the hot-gas loss q_2 recalculated through the static model at each perturbed value. (a) G1 (RETAL 45 t/h); (b) G2 (VU-40 235 t/h). Dotted lines indicate the nominal values; Figure S4: Monte Carlo propagation ($N = 2000$) of the inter-node damping factor ($\Delta T_{1,\max}/\Delta T_{2,\max}$) under simultaneous uncertainty in the three parameters identified by the OAT screening as most influential on the steam-side response—the controller time constant ($\tau \in [4,7]$ min, ≈ ±27% about the nominal $\tau = 5.5$ min), the thermal mass of the water/steam system (M_2, ±10% about its nominal value), and the flame emissivity ($\varepsilon \in [0.40, 0.50]$, ≈ ±11% about the nominal $\varepsilon = 0.45$), all sampled from independent uniform distributions, with the full dynamic model executed within each iteration, for blend M1. The resulting median damping factor is $F = 10.9$ (90% CI: 10.0–11.7) for G1 and $F = 7.4$ (90% CI: 6.8–8.1) for G2, consistent with the technology-clustered attenuation obtained for the twelve mixtures (≈10.9 for G1 and ≈7.4 for G2). (a) G1 (RETAL 45 t/h); (b) G2 (VU-40 235 t/h). Red line: median; dashed lines: 90% confidence interval. Figure S5: Sensitivity of the emergy sustainability index (ESI) ranking of the 12 ternary mixtures to a ±30% perturbation of the three biomass transformities, propagated through the emergy model (N = 4000). Box: interquartile

range; whiskers: 5th–95th percentiles; red markers: values obtained with the adopted transformities; dashed line: ESI = 5 threshold.

Author Contributions: Conceptualization, E.O.C.P. and Y.C.A.; methodology, Y.C.A. and R.J.B.; software, Y.C.A.; validation, R.J.B., J.P.Z.d.P. and F.A.C.V.; formal analysis, Y.C.A. and L.A.I.C.; investigation, E.O.C.P. and Y.C.A.; resources, J.R.-R.; data curation, L.A.I.C.; writing—original draft preparation, E.O.C.P. and Y.C.A.; writing—review and editing, R.J.B., J.P.Z.d.P., F.A.C.V., L.A.I.C. and J.R.-R.; visualization, Y.C.A. and L.A.I.C.; supervision, J.R.-R.; project administration, Y.C.A. All authors have read and agreed to the published version of the manuscript.

Funding: This research received no external funding.

Institutional Review Board Statement: Not applicable.

Informed Consent Statement: Not applicable.

Data Availability Statement: The original contributions presented in this study are included in the article/supplementary material. Further inquiries can be directed to the corresponding authors.

Conflicts of Interest: The authors declare no conflict of interest.

References

1. Demirbas, A. Potential applications of renewable energy sources, biomass combustion problems in boiler power systems and combustion related environmental issues. *Prog. Energy Combust. Sci.* **2005**, *31*, 171–192. [CrossRef]
2. McKendry, P. Energy production from biomass (part 1): Overview of biomass. *Bioresour. Technol.* **2002**, *83*, 37–46. [CrossRef] [PubMed]
3. Tillman, D.A. Biomass cofiring: The technology, the experience, the combustion consequences. *Biomass Bioenergy* **2000**, *19*, 365–384. [CrossRef]
4. Koppejan, J.; Van Loo, S. *The Handbook of Biomass Combustion and Co-Firing*; Routledge: London, UK , 2012.
5. Pippo, W.A.; Garzone, P.; Cornacchia, G. Agro-industry sugarcane residues disposal: The trends of their conversion into energy carriers in Cuba. *Waste Manag.* **2007**, *27*, 869–885. [CrossRef] [PubMed]
6. Kabeyi, M.J.B.; Olanrewaju, O.A. Bagasse electricity potential of conventional sugarcane factories. *J. Energy* **2023**, *2023*, 5749122. [CrossRef]
7. Cortes-Rodriguez, E.F.; Nebra, S.A.; Sosa-Arnao, J.H. Experimental efficiency analysis of sugarcane bagasse boilers based on the first law of thermodynamics. *J. Braz. Soc. Mech. Sci. Eng.* **2017**, *39*, 1033–1044. [CrossRef]
8. Arnao, J.S. First and second law to analyze the performance of bagasse boilers. *Int. J. Thermodyn.* **2011**, *14*, 51–58. [CrossRef]
9. Mo, Q.; Zhu, X.; Deng, C.; Cen, S.; Ye, H.; Wang, C.; Lu, W.; Chen, X.; Lin, X. Analysis on influencing factors and improvement of thermal efficiency of bagasse boilers based on performance test data. *Energy* **2023**, *271*, 127099. [CrossRef]
10. Reyes, Y.; Pérez, M.; Barrera, E.; Martínez, Y.; Cheng, K. Thermochemical conversion processes of *Dichrostachys cinerea* as a biofuel: A review of the Cuban case. *Renew. Sustain. Energy Rev.* **2022**, *160*, 112322. [CrossRef]
11. Pedroso, D.T.; Kaltschmitt, M. *Dichrostachys cinerea* as a possible energy crop—facts and figures. *Biomass Convers. Biorefinery* **2012**, *2*, 41–51. [CrossRef]
12. Naranjo, R.A.; Conesa, J.; Pedretti, E.F.; Romero, O.R. Kinetic analysis: Simultaneous modelling of pyrolysis and combustion processes of *Dichrostachys cinerea*. *Biomass Bioenergy* **2012**, *36*, 170–175. [CrossRef]
13. Bhuiyan, A.A.; Blicblau, A.S.; Islam, A.S.; Naser, J. A review on thermo-chemical characteristics of coal/biomass co-firing in industrial furnace. *J. Energy Inst.* **2018**, *91*, 1–18. [CrossRef]
14. Gutiérrez, A.S.; Eras, J.J.C.; Huisingh, D.; Vandecasteele, C.; Hens, L. The current potential of low-carbon economy and biomass-based electricity in Cuba. The case of sugarcane, energy cane and marabu (*Dichrostachys cinerea*) as biomass sources. *J. Clean. Prod.* **2018**, *172*, 2108–2122. [CrossRef]
15. Pellegrini, L.F.; de Oliveira, S., Jr. Exergy analysis of sugarcane bagasse gasification. *Energy* **2007**, *32*, 314–327. [CrossRef]
16. Kamate, S.; Gangavati, P. Exergy analysis of cogeneration power plants in sugar industries. *Appl. Therm. Eng.* **2009**, *29*, 1187–1194. [CrossRef]
17. Agbor, E.; Zhang, X.; Kumar, A. A review of biomass co-firing in North America. *Renew. Sustain. Energy Rev.* **2014**, *40*, 930–943. [CrossRef]
18. Gil, M.V.; Rubiera, F. Coal and biomass cofiring: Fundamentals and future trends. In *New Trends in Coal Conversion*; Elsevier: Amsterdam, The Netherlands, 2019; pp. 117–140. [CrossRef]
19. Codes, P.T. *PTC-4—Fired Steam Generators*; ASME: New York, NY, USA, 2013; pp. 4–1998.

20. *EN 12952-10:2002*; Water-Tube Boilers and Auxiliary Installations. British Standard: London, UK, 2002.
21. Barroso, J.; Barreras, F.; Amaveda, H.; Lozano, A. On the optimization of boiler efficiency using bagasse as fuel. *Fuel* **2003**, *82*, 1451–1463. [CrossRef]
22. Molina, D.L.; Vidal Medina, J.R.; Sagastume Gutiérrez, A.; Cabello Eras, J.J.; Lopez, J.A.; Hincapie, S.; Quispe, E.C. Multiobjective optimization of the energy efficiency and the steam flow in a bagasse boiler. *Sustainability* **2023**, *15*, 11290. [CrossRef]
23. Kotas, T.J. *The Exergy Method of Thermal Plant Analysis*; Paragon Publishing: Wiltshire, UK, 2012.
24. Dincer, I.; Rosen, M.A. *Exergy: Energy, Environment and Sustainable Development*, 2nd ed.; Elsevier/Newnes: Oxford, UK, 2012. [CrossRef]
25. Bejan, A.; Tsatsaronis, G.; Moran, M.J. *Thermal Design and Optimization*; John Wiley & Sons: Hoboken, NJ, USA, 1995.
26. Compton, M.; Rezaie, B. Sustainability Enhancement of a Biomass Boiler through Exergy Analysis. *Proceedings* **2017**, *2*, 159. [CrossRef]
27. Costa, V.; Tarelho, L.; Sobrinho, A. Mass, energy and exergy analysis of a biomass boiler: A portuguese representative case of the pulp and paper industry. *Appl. Therm. Eng.* **2019**, *152*, 350–361. [CrossRef]
28. Tsatsaronis, G.; Park, M.H. On avoidable and unavoidable exergy destructions and investment costs in thermal systems. *Energy Convers. Manag.* **2002**, *43*, 1259–1270. [CrossRef]
29. Li, C.; Gillum, C.; Toupin, K.; Donaldson, B. Biomass boiler energy conversion system analysis with the aid of exergy-based methods. *Energy Convers. Manag.* **2015**, *103*, 665–673. [CrossRef]
30. Vučković, G.D.; Vukić, M.V.; Stojiljković, M.M.; Vučković, D.D. Avoidable and Unavoidable Exergy Destruction and Exergoeconomic Evaluation of the Thermal Processes in a Real Industrial Plant. *Therm. Sci.* **2012**, *16*, S433–S446. [CrossRef]
31. Aboul-Enein, A.A.; Awadallah, A.E.; Solyman, S.M.; Ahmed, H.A. Green synthesis of carbon nanomaterials from sugarcane bagasse using bio-silica supported bimetallic nickel-based catalysts. *Fuller. Nanotub. Carbon Nanostruct.* **2022**, *30*, 767–776. [CrossRef]
32. Mameri, F.; Delacourt, E.; Morin, C.; Schiffler, J. 0D Dynamic Modeling and Experimental Characterization of a Biomass Boiler with Mass and Energy Balance. *Entropy* **2022**, *24*, 202. [CrossRef] [PubMed]
33. Gómez, M.; Porteiro, J.; Patiño, D.; Míguez, J. Eulerian CFD modelling for biomass combustion. Transient simulation of an underfeed pellet boiler. *Energy Convers. Manag.* **2015**, *101*, 666–680. [CrossRef]
34. Atsonios, K.; Zeneli, M.; Nikolopoulos, A.; Nikolopoulos, N.; Grammelis, P.; Kakaras, E. Calcium looping process simulation based on an advanced thermodynamic model combined with CFD analysis. *Fuel* **2015**, *153*, 370–381. [CrossRef]
35. Wang, C.; Liu, Y.; Zheng, S.; Jiang, A. Optimizing combustion of coal fired boilers for reducing NOx emission using Gaussian Process. *Energy* **2018**, *153*, 149–158. [CrossRef]
36. Carlon, E.; Schwarz, M.; Golicza, L.; Verma, V.K.; Prada, A.; Baratieri, M.; Haslinger, W.; Schmidl, C. Efficiency and operational behaviour of small-scale pellet boilers installed in residential buildings. *Appl. Energy* **2015**, *155*, 854–865. [CrossRef]
37. Odum, H.T. Emergy evaluation. In Proceedings of the International Workshop on Advances in Energy Studies: Energy Flows in Ecology and Economy, Porto Venere, Italy, 26–30 May 1998.
38. Odum, H.T. Self-organization, transformity, and information. *Science* **1988**, *242*, 1132–1139. [CrossRef] [PubMed]
39. Brown, M.T.; Ulgiati, S. Emergy analysis and environmental accounting. *Encycl. Energy* **2004**, *2*, 329–354. [CrossRef]
40. Brown, M.T.; Ulgiati, S. Updated evaluation of exergy and emergy driving the geobiosphere: A review and refinement of the emergy baseline. *Ecol. Model.* **2010**, *221*, 2501–2508. [CrossRef]
41. Brown, M.T.; Ulgiati, S. Emergy evaluations and environmental loading of electricity production systems. *J. Clean. Prod.* **2002**, *10*, 321–334. [CrossRef]
42. Ulgiati, S.; Brown, M.T. Quantifying the environmental support for dilution and abatement of process emissions: The case of electricity production. *J. Clean. Prod.* **2002**, *10*, 335–348. [CrossRef]
43. Hovelius, K.; Hansson, P.A. Energy-and exergy analysis of rape seed oil methyl ester (RME) production under Swedish conditions. *Biomass Bioenergy* **1999**, *17*, 279–290. [CrossRef]
44. Aghbashlo, M.; Tabatabaei, M.; Soltanian, S.; Ghanavati, H.; Dadak, A. Comprehensive exergoeconomic analysis of a municipal solid waste digestion plant equipped with a biogas genset. *Waste Manag.* **2019**, *87*, 485–498. [CrossRef] [PubMed]
45. Maes, D.; Van Passel, S. Advantages and limitations of exergy indicators to assess sustainability of bioenergy and biobased materials. *Environ. Impact Assess. Rev.* **2014**, *45*, 19–29. [CrossRef]
46. Rubio-González, A.; Rubio Rodríguez, M.; Roque Díaz, P. Valoración técnica y económica para el incremento de los parámetros del vapor en ingenios azucareros cubanos. *Cent. Azúcar* **2018**, *45*, 24–31.
47. Borges, R.J.; Iturralde Carrera, L.A.; Bastida, E.J.L.; García-Martínez, J.R.; Carrillo-Serrano, R.V.; Rodríguez-Reséndiz, J. Energy sustainability indicators for the use of biomass as fuel for the sugar industry. *Technologies* **2024**, *12*, 36. [CrossRef]
48. Soleh, M.; Ahmad, A.H.; Juangsa, F.B.; Darmanto, P.S.; Pasek, A.D. Impact of different kinds of biomass mixtures on combustion performance, interaction and synergistic effects in cofiring of coal and biomass in steam power plants. *Clean Energy* **2023**, *7*, 1136–1147. [CrossRef]

49. Fernando, R. Cofiring high ratios of biomass with coal. *IEA Clean Coal Cent.* **2012**, *300*, 194.
50. Cavalcanti, E.J.; Carvalho, M.; da Silva, D.R. Energy, exergy and exergoenvironmental analyses of a sugarcane bagasse power cogeneration system. *Energy Convers. Manag.* **2020**, *222*, 113232. [CrossRef] [PubMed]
51. Lythcke-Jørgensen, C.; Haglind, F.; Clausen, L.R. Exergy analysis of a combined heat and power plant with integrated lignocellulosic ethanol production. *Energy Convers. Manag.* **2014**, *85*, 817–827. [CrossRef]
52. Edrisi, S.A.; Sahiba, S.A.; Chen, B.; Abhilash, P. Emergy-based sustainability analysis of bioenergy production from marginal and degraded lands of India. *Ecol. Model.* **2022**, *466*, 109903. [CrossRef]
53. Ren, S.; Feng, X.; Yang, M. Emergy evaluation of power generation systems. *Energy Convers. Manag.* **2020**, *211*, 112749. [CrossRef]

Disclaimer/Publisher's Note: The statements, opinions and data contained in all publications are solely those of the individual author(s) and contributor(s) and not of MDPI and/or the editor(s). MDPI and/or the editor(s) disclaim responsibility for any injury to people or property resulting from any ideas, methods, instructions or products referred to in the content.